

CREEP OF COMPACTS OF COLLOIDAL  
BOEHMITE (AlOOH) DURING DEHYDROXYLATION

by

ROBERT GUSTAVE ST-JACQUES  
B.A., B.A.Sc. (METALLURGY), University of Montreal

A THESIS SUBMITTED IN PARTIAL FULFILMENT  
OF THE REQUIREMENTS FOR THE DEGREE OF  
MASTER OF APPLIED SCIENCE

in the Department

of

METALLURGY

We accept this thesis as conforming to the  
standard required from candidates for  
the degree of Master of Applied Science

Members of the Department  
of Metallurgy

THE UNIVERSITY OF BRITISH COLUMBIA

November, 1968

In presenting this thesis in partial fulfilment of the requirements for an advanced degree at the University of British Columbia, I agree that the Library shall make it freely available for reference and Study.

I further agree that permission for extensive copying of this thesis for scholarly purposes may be granted by the Head of my Department or by his representatives. It is understood that copying or publication of this thesis for financial gain shall not be allowed without my written permission.

Department of Metallurgy  
The University of British Columbia  
Vancouver 8, Canada

Date November 27<sup>th</sup> 1968

ABSTRACT

A compressive creep study of cold compacted colloidal boehmite has been carried out during the dehydroxylation reaction. The creep tests were made as a function of temperature, applied stress and the relative density of the cold compact. The activation energy for creep has been found to be  $9.1 \pm 1.5$  Kcal/mole. The total creep rate was due to the stress associated with the neck formation at the points of contact and the applied stress. The creep rate is proportional to the applied stress. The final form of the total creep rate equation is  $\dot{\epsilon} = [0.144 \exp\left(\frac{-9,100 \pm 1,500}{RT}\right) + 2.2 \times 10^{-7} \sigma] \text{ sec}^{-1}$ . Electron photomicrographs of fractured surfaces of deformed specimens revealed the presence of contact points in the aligned fibers, confirming the existence of the driving force for shrinkage. Equations relating the change in length and the strength of a compact with time have been tested with the experimental data, which indicated that the rate controlling mechanism may be volume diffusion for the creep process.

ACKNOWLEDGEMENTS

The author wishes to acknowledge the help given by Dr. A.C.D. Chaklader throughout this work. Thanks are also extended to the staff of the Department of Metallurgy for their advice. Financial aid provided by the National Research Council and by the Quebec Ministry of Education is gratefully acknowledged.

TABLE OF CONTENTS

	<u>PAGE</u>
I. INTRODUCTION . . . . .	1
I.1 Reactive hot-pressing and its importance to the ceramic industry . . . . .	1
I.2 Phenomenological explanation for enhanced compaction . . . . .	3
I.3 Previous studies of deformation during phase transformations . . . . .	3
I.4 Previous studies of reactive hot-pressing of Boehmite (AlOOH) . . . . .	5
I.5 Explanation for enhanced compaction of Boehmite . . .	9
I.6 Objective of this work . . . . .	10
II. EXPERIMENTAL TECHNIQUES AND RESULTS . . . . .	11
II.1 Material . . . . .	11
a) Description . . . . .	11
b) Preparation of compacts . . . . .	14
II.2 Equipment . . . . .	16
II.3 Creep at a constant heating rate . . . . .	16
II.4 Creep under isothermal conditions . . . . .	18
II.5 Creep under different stresses . . . . .	20
II.6 Density dependence of creep . . . . .	26
II.7 Complementary experimental work . . . . .	26
a) Creep tests with Kaolinite . . . . .	26
b) Electron microscopy study . . . . .	26
c) Weight loss vs. shrinkage . . . . .	26
d) Measurements of specific surface areas . . . . .	27
e) Compressive strength of the compacts . . . . .	27

TABLE OF CONTENTS (continued)

	<u>PAGE</u>
III. DISCUSSION . . . . .	36
III.1 Effect of the soaking time . . . . .	36
III.2 Creep due to surface tension . . . . .	39
III.3 Neck formation . . . . .	40
III.4 Effect of the density on the creep rate . . . . .	41
III.5 Particle deformation . . . . .	41
III.6 Phenomenological equation of the creep rate . . . . .	43
III.7 Equation relating the change of length of the compacts with time . . . . .	50
III.8 Strength of the compacts as a function of time . . . . .	54
IV. SUMMARY AND CONCLUSIONS . . . . .	60
V. SUGGESTIONS FOR FUTURE RESEARCH . . . . .	61
VI. APPENDIX - Expansion correction . . . . .	62
VII. REFERENCES . . . . .	65

LIST OF FIGURES

<u>NO.</u>		<u>PAGE</u>
1	Translucent $\gamma$ -Al <sub>2</sub> O <sub>3</sub> sheet made by reactive hot pressing . . . . .	2
2	A schematic model of interparticle bonding with deformation . . . . .	4
3	Compaction curves of Boehmite . . . . .	8
4	Transmission electron micrographs of boehmite powder.	12
5	Structure of Boehmite showing atomic arrangement . .	13
6	Weight of powder and applied pressure vs. fractional density of the compacts . . . . .	15
7	Schematic diagram of furnace and loading assembly . .	17
8	Effect of applied stress on creep at a constant heating rate, 27°C/minute during dehydroxylation . .	19
9	Creep at different temperatures under 265 psi . . . .	21
10	Creep at 500°C, under 265 and zero psi . . . . .	22
11	Stress dependence of creep at 350°C . . . . .	23
12	Stress dependence of creep at 400°C . . . . .	24
13	Stress dependence of creep at 550°C . . . . .	25
14	Fractional density dependence of creep at 400°C . . .	28
15	Fractional density dependence of creep at 500°C . . .	29
16	Creep of Kaolinite . . . . .	30
17	Replica electron micrographs of fractured surface of boehmite compact after dehydroxylation . . . . .	31
18	Creep at 500°C, under 265 psi and after different soaking times . . . . .	37
19	Creep, fraction decomposed and specific surface area at 500°C, as a function of time . . . . .	38
20	Creep rate as a function of fractional density . . .	42
21	Creep rate as a function of stress at different temperatures . . . . .	44

LIST OF FIGURES (continued)

<u>NO.</u>		<u>PAGE</u>
22	Log $\dot{\epsilon}_s$ as a function of log $\sigma$ . . . . .	45
23	Log of creep rates as a function of the reciprocal of the absolute temperature . . . . .	47
24	Log $\left\{\frac{L}{L_0} \left[1 - \left(\frac{L}{L_0}\right)^{1/3}\right]\right\}$ as a function of log time . . . . .	55
25	Log strength as a function of log time . . . . .	59
26	Net dilatation of the specimen holding frame . . . . .	63
27	Net dilatation of specimen holding frame and corrected creep curves . . . . .	64

LIST OF TABLES

<u>NO.</u>		<u>PAGE</u>
I	Stress dependence of the creep rate . . . . .	33
II	Fractional density dependence of the creep rate . . .	33
III	Fraction reacted as a function of time . . . . .	34
IV	Specific surface area as a function of time . . . . .	34
V	Compressive strength of specimens after dehydroxy- lation . . . . .	35
VI	Coefficients of the phenomenological equation of the creep rate . . . . .	48

## I. INTRODUCTION

### I.1 REACTIVE HOT-PRESSING AND ITS IMPORTANCE TO THE CERAMIC INDUSTRY

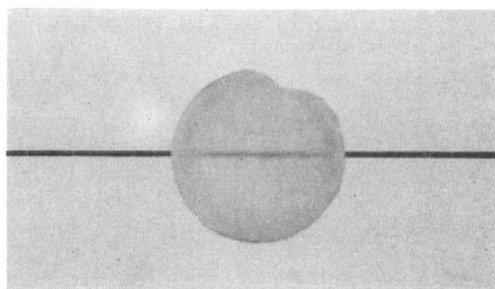
Reactive hot-pressing is a process by which powdered materials can be densified, at much lower temperatures and in shorter periods than conventionally used.

This process is essentially a hot pressing technique which is carried out in conjunction with either a polymorphic transformation or a decomposition reaction. The application of pressure during such a transformation or a decomposition reaction can produce considerable interparticle bonding, resulting in the formation of a strong and dense body.

In order to obtain translucent alumina for example, it is normally necessary<sup>(1)</sup> to hot-press alumina powder under 6000 psi at 1500°C for a period of 2 to 5 hours. By pressing aluminum hydroxide during its dehydroxylation reaction (350°C - 550°C), however, a translucent alumina sheet can be produced after 10 minutes under 15,000 psi at 500°C (Figure 1).

The application of pressure during the polymorphic transformation of non-stabilized zirconia powder (1160 - 1205°C) has been found<sup>(2)</sup> to be a very effective method of fabricating very dense and strong non-stabilized zirconia products instead of the normal hot-pressing process at 1800°C.

When compared to the conventional hot-pressing technique, reactive hot pressing presents the advantages of shorter time, much lower temperatures



X2½

Figure 1 : Translucent  $\gamma$ - $\text{Al}_2\text{O}_3$  sheet produced by Reactive Hot-Pressing at 500°C/10 mins.

Thickness : 0.04 inch.

and consequently the possibility of using higher pressures.

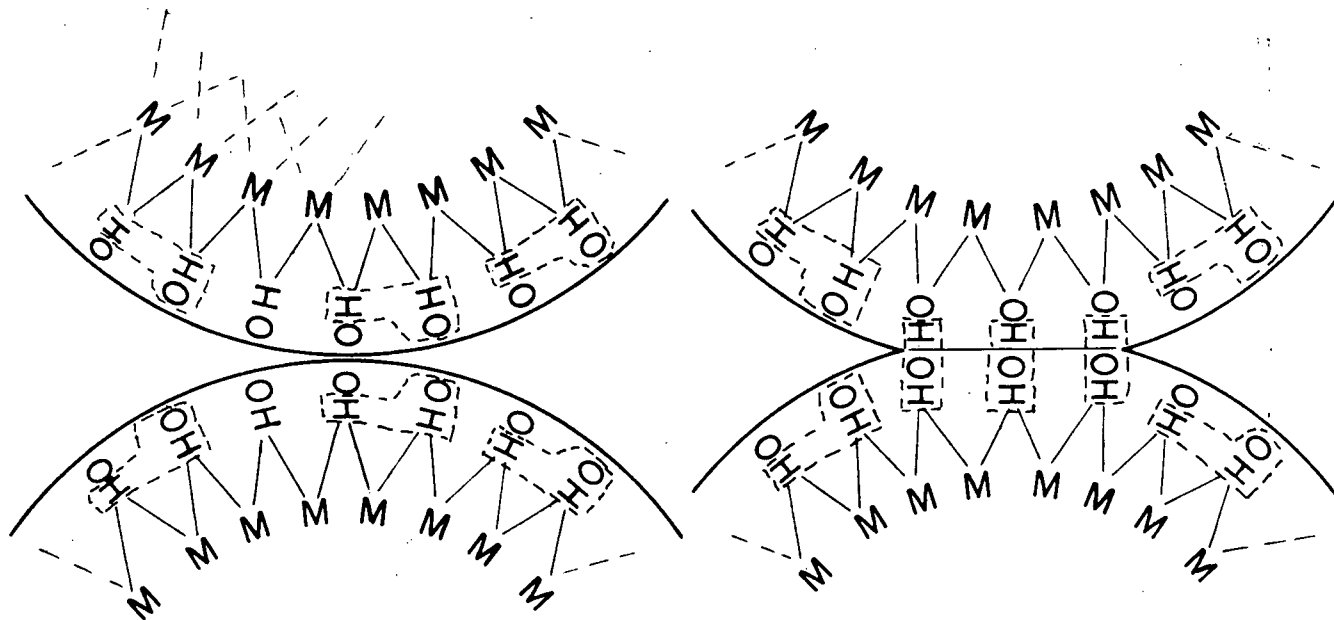
## I.2 PHENOMENOLOGICAL EXPLANATION FOR ENHANCED COMPACTION

Enhanced compaction of a powder compact during either a decomposition reaction or a polymorphic phase transformation has been reported by several workers<sup>(3)</sup>. The process of reactive hot-pressing utilizes the fact that the reactivity of a solid is considerably enhanced during phase transformations, decomposition, or dissociation reactions (the Hedvall effect)<sup>(4)</sup>. It is suggested that broken bonds and unsatisfied valence links may exist both on the surface and in the bulk of the particles of a solid during a decomposition reaction; these may be available for interfacial reaction leading to inter-particle bonding<sup>(5)</sup>. Moreover, very transient instability of the atomic position during a reaction can produce a transient plastic state which may be utilized for densification (Figure 2).

Interparticle bonding can be achieved by relinking the broken bonds across the interface. However to explain the elimination of pores or voids from the compact it is necessary to postulate a mechanism involving material transport. If there is a plastic state during the reaction, the material can flow easily and this may result in densification.

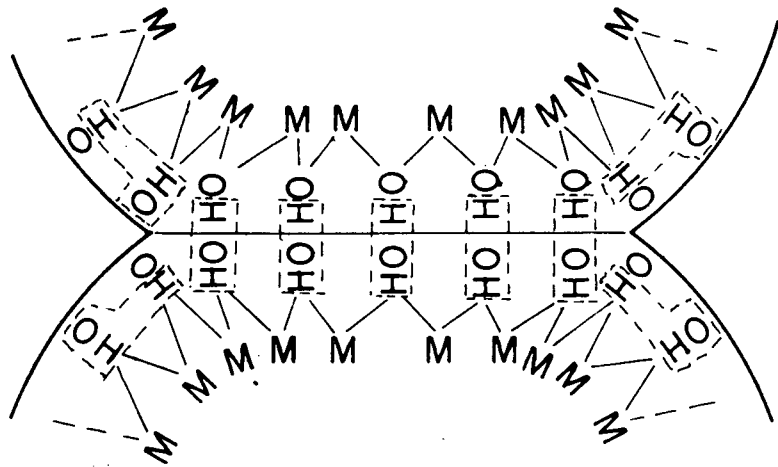
## I.3 PREVIOUS STUDIES OF DEFORMATION DURING PHASE TRANSFORMATIONS

Unusual ductility effects have been observed in studies of mechanical deformation during phase transformations of metallic materials<sup>(6)</sup>. Similar effects would also be expected in other crystalline structures such as ceramic oxides. Observations on plastic behaviour in quartz



NO INTERPARTICLE BONDING

INTERPARTICLE BONDING  
WITHOUT DEFORMATION.



INTERPARTICLE BONDING WITH  
DEFORMATION.

Figure 2 : A Schematic Model of Interparticle Bonding with Deformation.

crystals during the  $\alpha$  to  $\beta$  phase change have been reported by Chaklader<sup>(7)</sup>, while Hart<sup>(8)</sup> in an investigation of creep deformation in pure zirconia, using a creep-in-bending method with programmed temperature increase, showed the occurrence of superplasticity or transformation plasticity at temperatures near the monoclinic to tetragonal phase transformation. Also, Morgan and Scala<sup>3,C)</sup> have prepared high density oxide ceramics from hydroxides by application of pressure during the dehydroxylation reaction and showed that phase changes, accompanying chemical reactions, can aid the sintering process, especially under applied pressure. Utilization of this phenomenon allowed them to fire at temperatures much lower than those used previously.

A study by Sunderland and Chaklader<sup>(9)</sup> of the neck growth between tips of single crystals of  $\text{Ca}(\text{OH})_2$  and between two hemispherical tips of compacted  $\text{Mg}(\text{OH})_2$  has shown both deformation and interaction at the contact point during dehydroxylation reaction.

The kinetics of compaction during the dehydroxylation reaction of china clay, fireclay, magnesium hydroxide and aluminum hydroxide have been studied by Cook and Chaklader<sup>(10)</sup>. They concluded that the true mechanism or mechanisms of compaction cannot be determined solely by kinetic analysis, although it can be assumed that the enhanced compaction is dependent on the dehydroxylation reaction and other phase changes occurring in the material.

#### I.4 PREVIOUS STUDIES OF REACTIVE HOT-PRESING OF BOEHMITE (AlOOH)

McKenzie and Chaklader<sup>(5)</sup> made the first attempt to establish

a relation between the strength or bulk density of a boehmite compact and the extent of the dehydroxylation reaction occurring during the densification process under reactive hot-pressing conditions. The results were analyzed using the empirical relation that the strength is proportional to the extent of reaction. It was assumed that at each hot-pressing condition both the reaction and strength resulting from the interparticle bond formation, reached a pseudo-equilibrium state.

The temperature coefficient of the reaction can be determined provided an equilibrium condition is attained and this should permit a value for the enthalpy of the reaction to be obtained. The energy values obtained from the analysis of the data were smaller than the enthalpy values reported by other workers for the reaction concerned. However, in view of the fact that the standard state of this reaction was not known and the uncertainty of the assumption that the strength at any stage was proportional to the extent of reaction, this disagreement was not unexpected. Nevertheless, the results showed that densification was directly related to the reaction involved and that the compaction behavior during the dehydroxylation reaction was significantly different from the compaction behavior after the reaction.

In order to substantiate this further, attempts were made by Cook and Chaklader<sup>(10)</sup> to study the kinetics of compaction during the dehydroxylation process. Initial experiments under isothermal conditions did not permit useful conclusions to be made for the following reasons:

a) At high temperatures, the dehydroxylation reaction took place within

- a few minutes and the creep rate was too fast to be measured accurately.
- b) The compaction rate was very sensitive to the size of the specimen as this controlled the volume of vapor phase formed during the reaction.
  - c) The rate of vapor phase removal could be controlled by varying the annular space between the die wall and the plungers and this also affected the rate of compaction.
  - d) At higher temperatures, when a significant portion of the dehydroxylation reaction was completed during the heating-up period, the study of compaction rate produced erroneous and nonreproducible results.

For these reasons, Cook and Chaklader evaluated the compaction kinetics by studying the compaction behavior over a range of constant heating rates.

In the work of Cook and Chaklader, the powder was pressed under a constant pressure of 5000 psi in a cylindrical die and the compaction was recorded as the temperature was increased. Figure 3 shows the compaction curves replotted from Cook's data together with a thermogravimetric (TGA) plot of the same material for comparison.

The similarity between the compaction curves and the TGA plot is quite apparent. Between 350°C and 550°C there was a significant weight loss (15%) and about 8% compaction was obtained during this period. This range of temperature corresponds to the dehydroxylation of boehmite. The temperature gradient from the surface to the core of the compact caused the surface to reach the dehydroxylation temperature

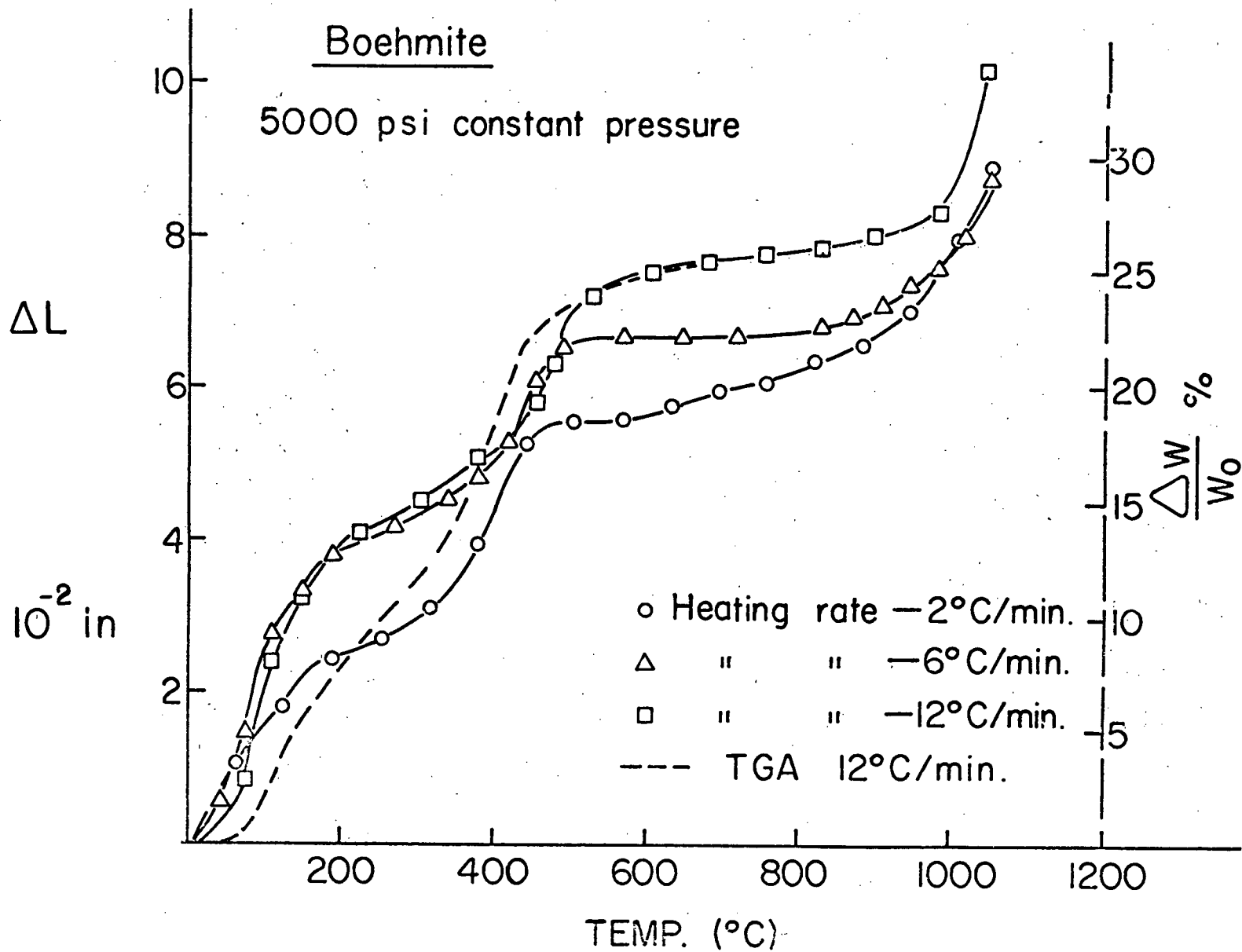


Figure 3: Compaction curves of Boehmite.

range before the core. With a slow heating rate, there was sufficient dehydroxylation at the surface to produce a hard cylindrical sleeve while the center was still unreacted. This rigid material slowed the compaction at low heating rates as shown in Figure 3.

In addition to compaction during the decomposition reaction, additional enhanced compaction was also obtained during the  $\gamma$ -alumina to  $\alpha$ -alumina phase change at  $1100^{\circ}\text{C}$ .

#### I.5 EXPLANATION FOR ENHANCED COMPACTION OF BOEHMITE

Morgan and Scala<sup>(3,C)</sup> claimed that on raising the temperature to the decomposition range, densification occurs by a complex superimposition of chemically induced fragmentation and mechanical rearrangement of newly formed, very fine oxide grains (generated from the hydroxide). They reported that water vapor given off during this first stage probably continues to activate further sintering of the oxide mass and at the end of the reaction escapes, leading to the theoretical density and translucency.

Cook and Chaklader<sup>(10)</sup> suggested that in the dehydroxylation process, interaction between (OH) ions to form  $\text{H}_2\text{O}$  molecules and subsequent diffusion of these molecules does not involve any large scale particle movement. In order to explain the densification of particulate compacts in the presence of an applied stress, large scale particle rearrangement must exist. They concluded that fragmentation during the dehydroxylation process may also significantly affect the particle flow.

## I.6 OBJECTIVE OF THIS WORK

In order to understand the compaction mechanisms during reactive hot-pressing of hydroxides, a programme of research was undertaken to study the flow behavior of powder compacts during the dehydroxylation reaction. This work forms a part of that programme. The flow behavior of cold compacted cylindrical specimens of fibrillar colloidal boehmite was investigated by compression creep tests under isothermal conditions.

## II EXPERIMENTAL TECHNIQUES AND RESULTS

### II.1 MATERIAL

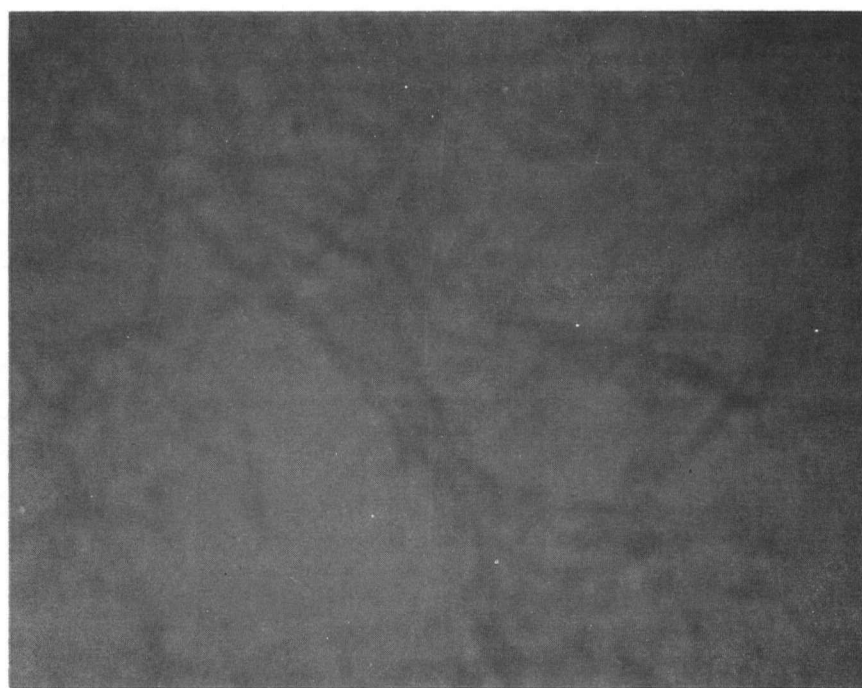
#### a) Description

The material used in this study was colloidal boehmite supplied by E.I. du Pont de Nemours and Company under its trade-mark name of Baymal. The characteristics of the powder are described by Iler<sup>(11)</sup> as having AlOOH, 83.1%; acetate as acetic acid, 9.8%; chemically bound water, 3.3%; physically adsorbed water, 1.8%; sulphate as SO<sub>4</sub>, 1.7%. The true density of the material is 2.28 grams per cc. The particles are fibrillar, being about 50 angstroms in diameter and 1000 to 2000 angstroms long. Figures 4(a) and 4(b) show transmission electron photomicrographs of the powder. Specimens for the electron microscope were prepared by dispersing AlOOH in distilled water and then transferring it to a carbon support film placed on a copper grid. The water was evaporated off and the copper grid was placed in the electron microscope. Figure 4(b) shows fibers in a more dispersed state than Figure 4(a). The powder consists of discrete fibers in the form of loosely associated porous aggregates.

The dehydroxylation of boehmite to gamma alumina involves only a minor change in the over-all crystal structure. The structure of boehmite<sup>(12)</sup> consists of oxygen ion layers that do not fit with each other but within which the oxygen ions are in cubic packing. The OH directions form zig-zag chains between the planes of the oxygen ions. Figure 5 shows the a-plane and the c-plane of a model of boehmite. When the hydroxyl ions are removed, the layers form a cubic close-packed arrangement of oxygen ions with the smaller aluminum ions remaining in

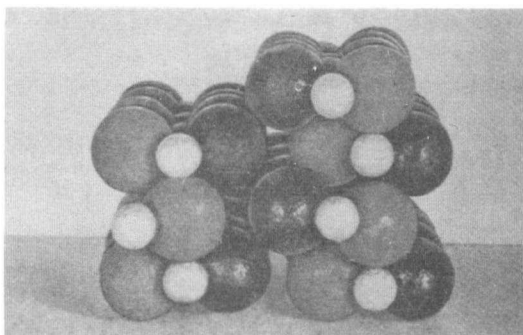


(a) X40,000

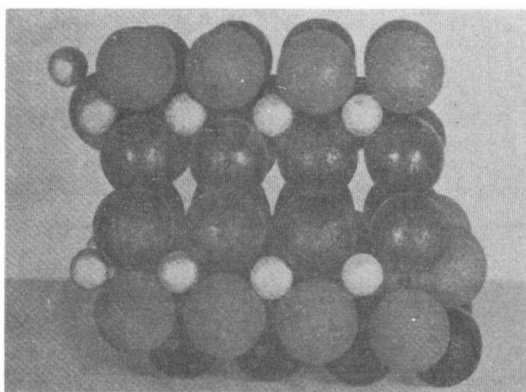


(b) X120,000

Figure 4 : Transmission electron micrographs of boehmite powder.



"a" plane



"c" plane

Figure 5 : Structure of boehmite showing atomic arrangement.

Glossy black balls : Hydroxyl Ions.  
Large gray balls : Oxygen Ions.  
Small balls : Aluminum Ions.

a random arrangement in the interstitial sites.

The formula  $\text{AlOOH}$  gives a proportion of 2 to 1 between the hydroxyl ions and the aluminum atoms. However the aluminum ions lying at the surface of the boehmite fibers would be subjected to cationic screening and would pick up hydroxyl groups in order to become stable. Because the surface area is large ( $250 \text{ m}^2/\text{gram}$ ), these hydroxyl groups are responsible for a measurable excess of water over the formula  $\text{AlOOH}$ . This chemically bound water is distinct from the physically adsorbed water. Iler found that the chemically bound water plus the acetate corresponded closely to the theoretical amount required to cover the surface with OH groups and acetic acid. He reported also that when the powder is heated up to  $300^\circ\text{C}$ , the acetate and adsorbed water are removed.

#### II.1 b) Preparation of Compacts

The powder was cold-pressed in a cylindrical die to form compacts 0.190 inch in diameter and 0.270 - 0.280 inch long. The weight of the powder and the load applied on the ram during the fabrication was varied to obtain compacts of different densities but of the same length. Figure 6 shows the weight of the powder and the pressure applied to form the compacts as a function of the green density. To ensure identical compaction rate, the compacts were cold-pressed at 0.1 inch per minute in an Instron machine. Three batches of compacts, each of 50 pellets, were prepared in this manner.

The densities of the compacts were calculated from weight to volume ratio. It was observed that the compacts having less than 0.50 fractional density were too fragile to handle and that compacts of more

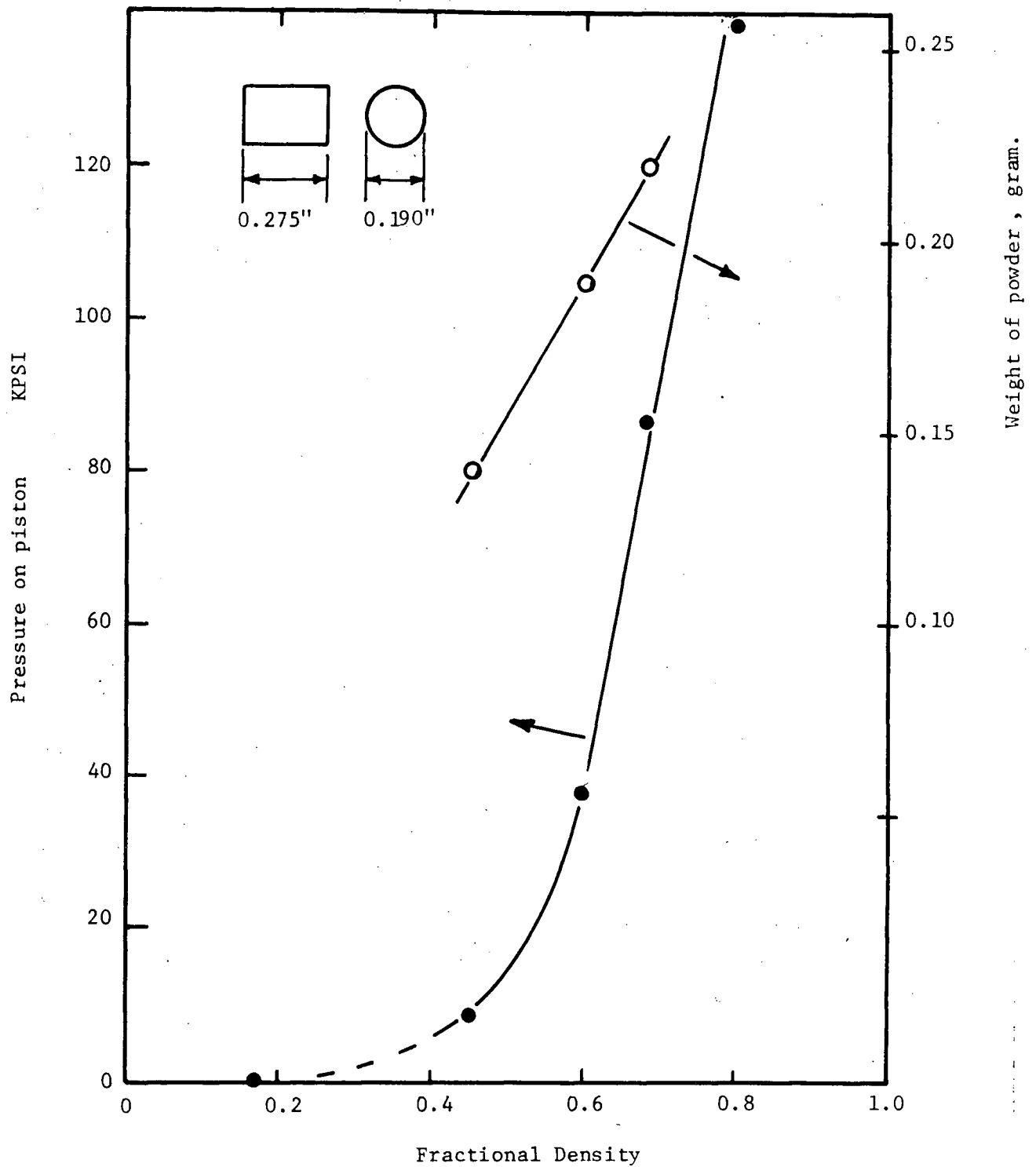


Figure 6: Relation between pressure on piston, weight of powder and fractional density of pellets having constant dimensions.

than 0.65 fractional density were strong but very difficult to release intact from the die due to friction. Hence, most of the experiments have been performed with compacts of 0.60 fractional density.

## II.2 EQUIPMENT

The apparatus used in the creep study has been built by Sunderland<sup>(9)</sup> and is shown in Figure 7. It consisted of a horizontal resistance vacuum furnace in which a pressure of  $<5 \times 10^{-3}$  torr was maintained. The vacuum chamber was water cooled and the spring loading device laid outside the heating zone. The loading frame and the ram were made of stainless steel. The furnace could be programmed for constant heating rates or could be used for isothermal creep tests. The temperature of the specimen was recorded by a chromel-alumel thermocouple touching its surface. The same thermocouple was used to control the temperature in conjunction with a Honeywell controller. An additional thermocouple was occasionally used to measure the temperature of the interior of the specimen in order to determine the temperature distribution during the creep study. The linear dimensional change was measured by a dial indicator (sensitivity : 0.0001 inch) and was plotted as a function of the time to give the creep rate. A transducer was also available to record directly the dimensional change on a strip-chart recorder; however, the non-linearity of the transducer voltage over a large range of ram displacement prevented its use.

## II.3 CREEP AT A CONSTANT HEATING RATE

The cylindrical specimen was placed loosely between the loading frame and the ram and the system was pumped down to  $5 \times 10^{-3}$  torr. A

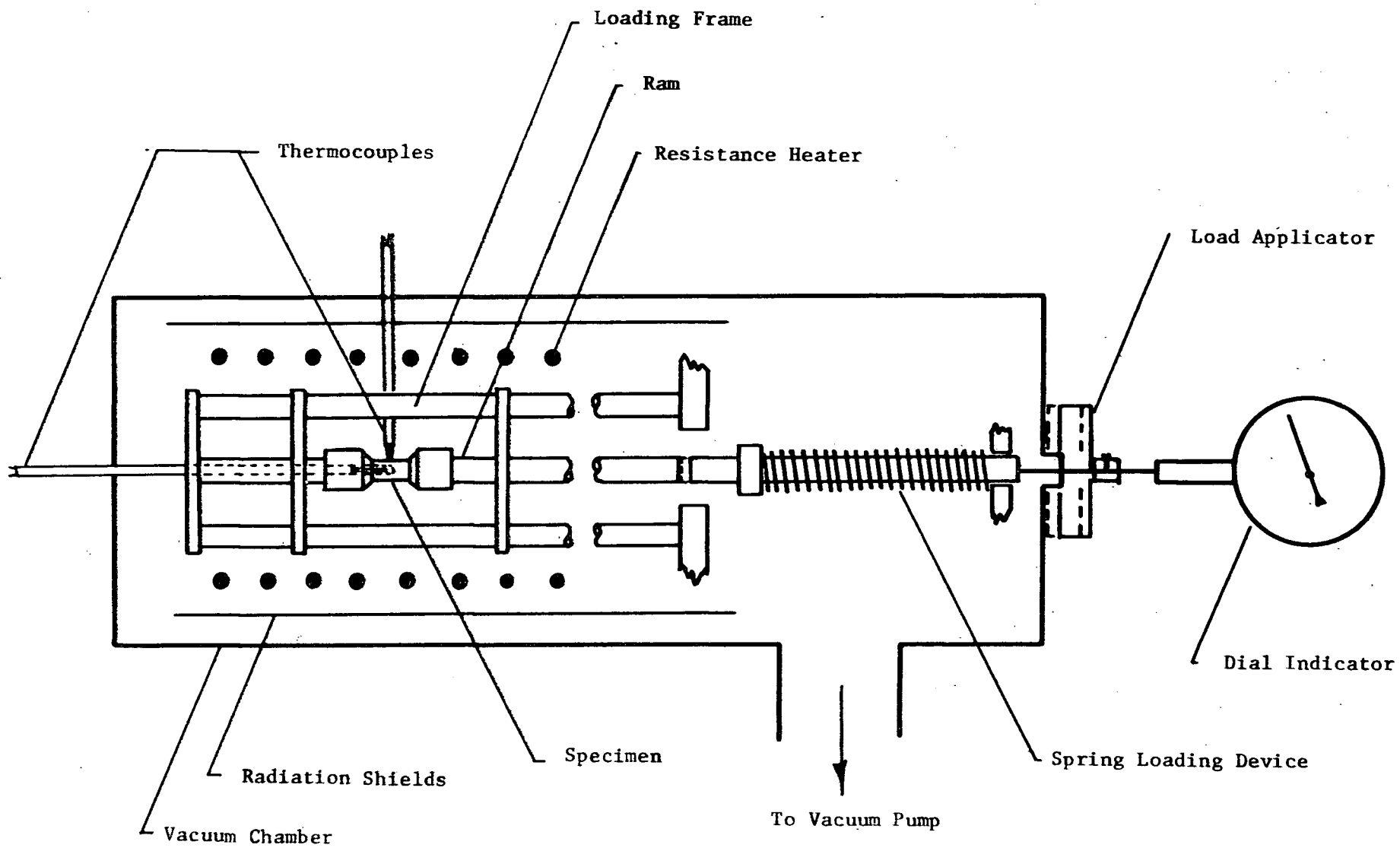


Figure 7 : Schematic diagram of furnace and loading assembly.

stress of 105 psi was then applied and the specimen was heated at a rate of either 27 or 2°C per minute. The creep data obtained was subsequently corrected for the expansion of the holding frame (Appendix I).

No significant difference was observed between the total creep when tests were made under the same stress (105 psi) but at different heating rates (2 and 27°C per minute). However, both the creep rate and the total creep increased with increased stress (155 psi) as shown in Figure 8.

#### II.4 CREEP UNDER ISOTHERMAL CONDITIONS

The compact was heated in vacuum at the maximum heating rate obtainable (200°C per minute) until the surface temperature had reached the test temperature. By placing a thermocouple inside the specimen, it was found that the inside of the specimen took an extra 30 seconds to reach the test temperature but that thereafter there was less than a 10°C temperature differential between the outside and the inside of the specimen. It was accordingly decided to apply the load 30 seconds after the thermocouple touching the surface of the compact had reached the test temperature. Creep tests were carried out at five temperatures: 350, 400, 450, 500 and 550°C. The duration of the tests varied from 10 to 20 minutes, depending on the test temperature. However, several experiments were carried out for periods up to one hour.

As previously noted the load was applied 30 seconds after the test temperature was reached. Accordingly at 350°C, the load was applied 3 minutes after the power was turned on and at 550°C it was

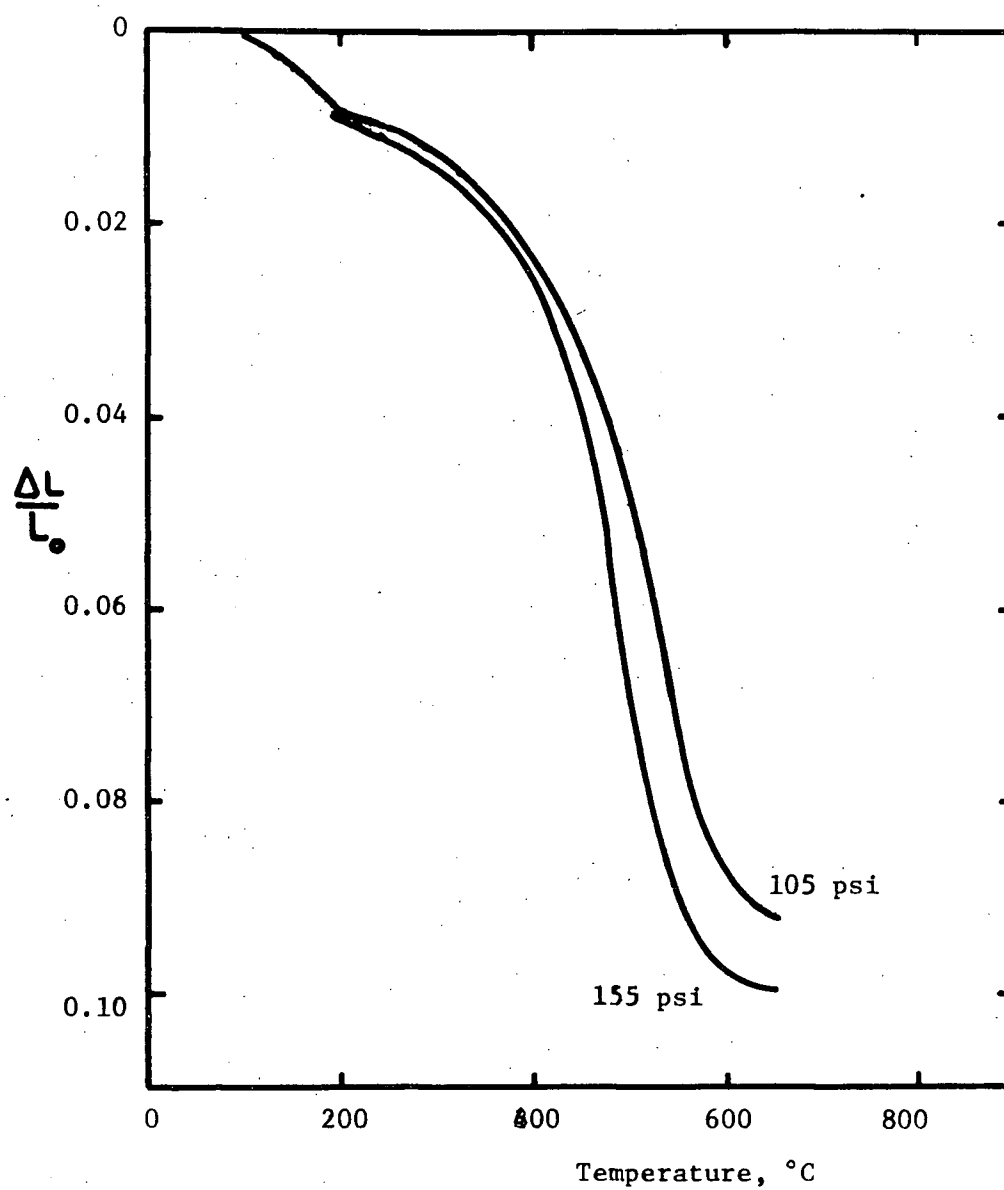


Figure 8 : Effect of applied stress on creep at a constant heating rate of 27°C per minute.

applied after  $4\frac{1}{2}$  minutes. This explains why in Figure 9 the origin of the different curves shifted to an increasing time as the test temperature increased. However, the fact that the curves originate at a point where  $\frac{\Delta L}{L_0}$  is different from zero indicates that the compacts shrank even without any applied stress. With an applied stress of 265 psi, the creep rate increased from  $11 \times 10^{-5} \text{ sec}^{-1}$  at  $350^\circ\text{C}$  to  $48 \times 10^{-5} \text{ sec}^{-1}$  at  $550^\circ\text{C}$ . After 1600 seconds at  $350^\circ\text{C}$  or 800 seconds at  $550^\circ\text{C}$  the creep rates approached zero.

#### II.5 CREEP UNDER DIFFERENT STRESSES

By changing the spring of the loading device, stresses of 31, 61, 105, 155 and 265 psi could be applied. The spring loading device was calibrated in an Instron testing machine to  $\pm 0.05$  lb.

To find if there is any shrinkage when the compact undergoes dehydroxylation (i.e. free of applied stress) a series of specimens were heated under vacuum at  $350^\circ\text{C}$  or  $500^\circ\text{C}$  over different periods and the dimensional change was determined.

The effect of the applied stress is shown in Figure 10. It is quite evident from this figure that there is creep without any applied stress. At  $500^\circ\text{C}$ , the creep rate increased from  $21 \pm 2$  to  $31 \pm 2 \times 10^{-5} \text{ sec.}^{-1}$  under 265 psi. Figure 11, 12 and 13 show some typical creep curves at  $350^\circ\text{C}$ ,  $400^\circ\text{C}$  and  $550^\circ\text{C}$  respectively. The creep curves become linear 10 - 15 seconds after the load is applied. This transient creep was observed in most experiments and is believed to be an adjustment period for the distribution of stress on the whole specimen. This part of the creep has not been taken into consideration in the creep

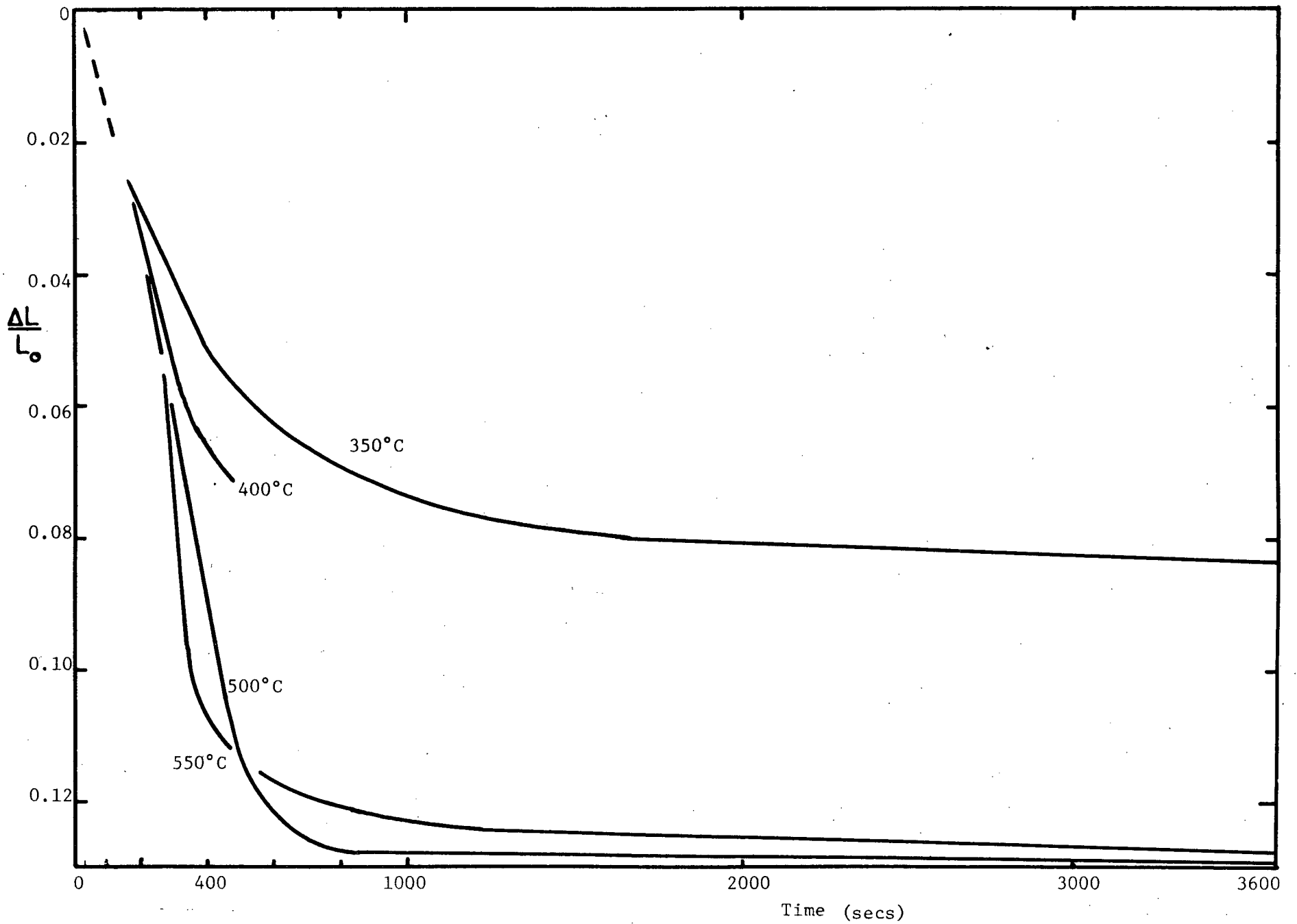


Figure 9 : Creep at different temperatures under 265 psi.

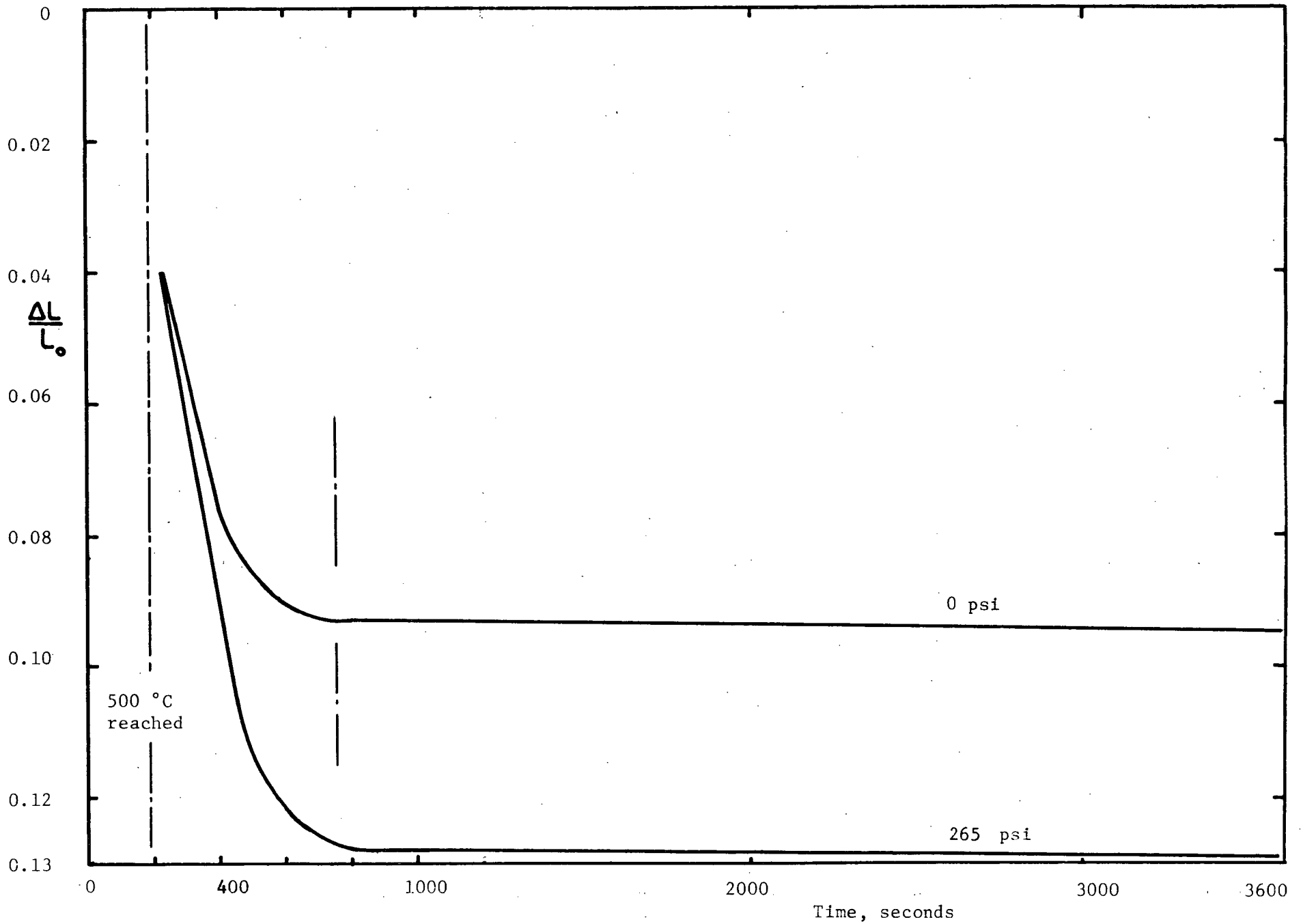


Figure 10 : Creep at 500°C, under 265 and zero psi.

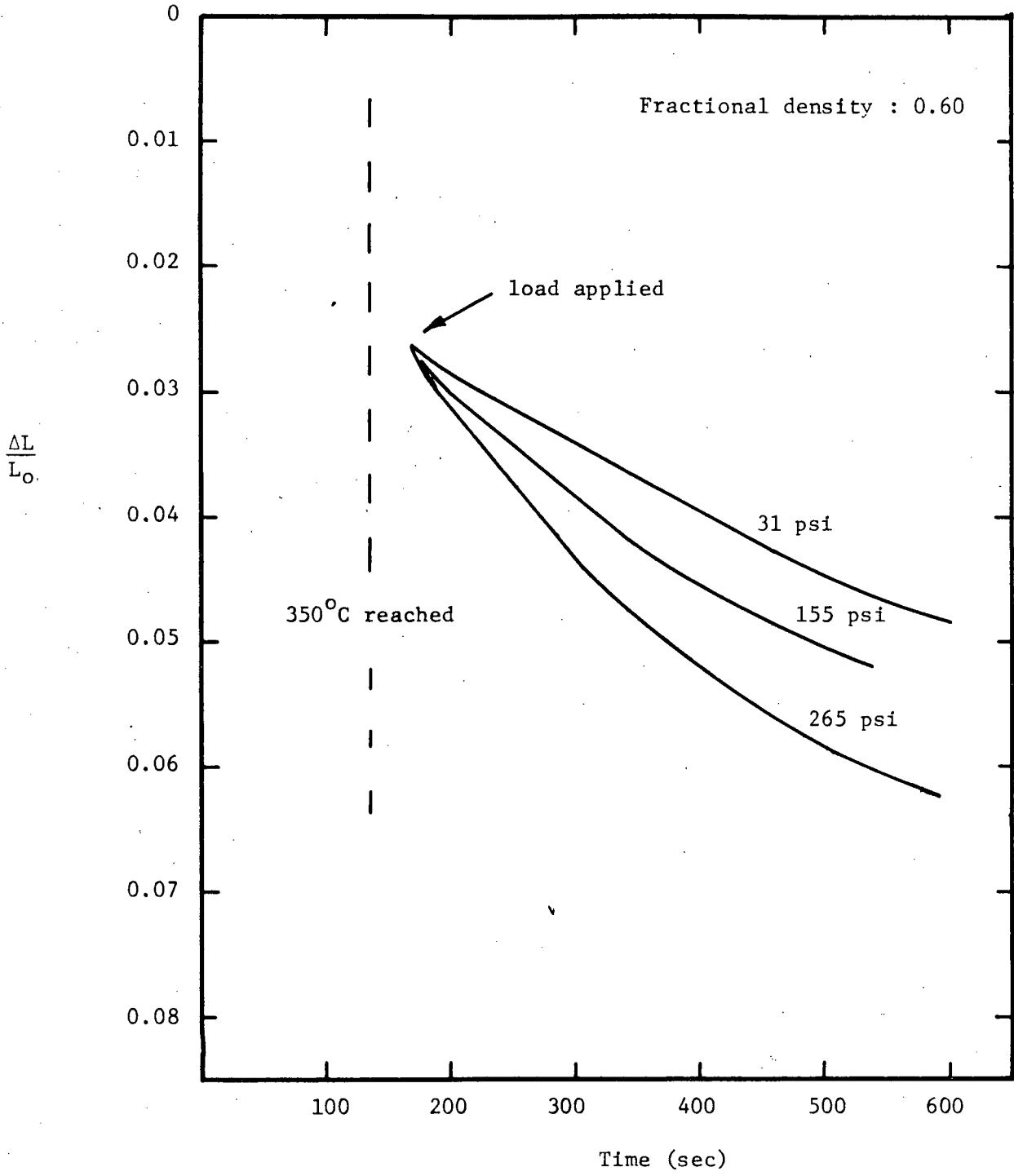


Figure 11 : Stress dependence of Creep at 350°C

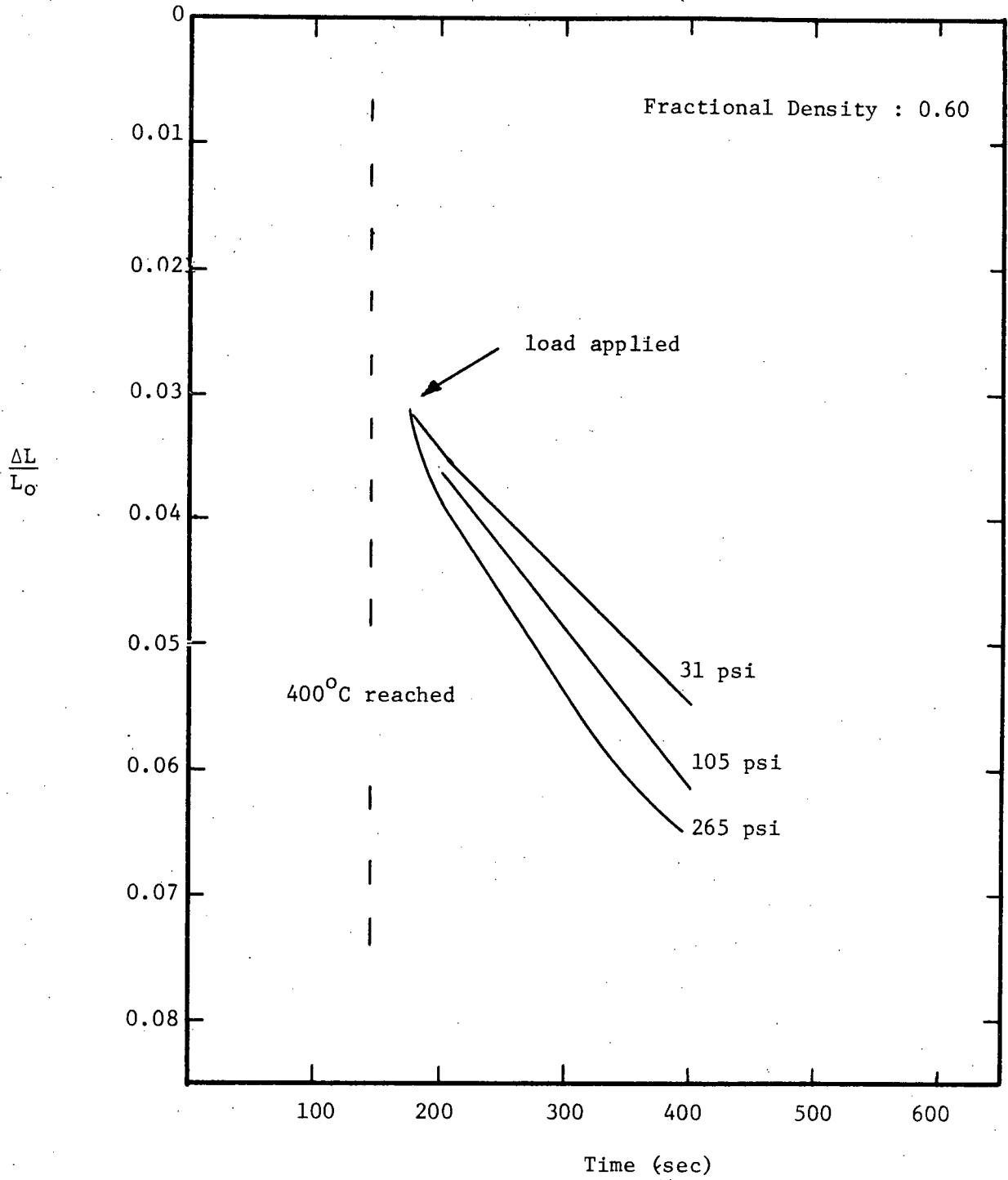


Figure 12 : Stress Dependence of Creep at 400°C

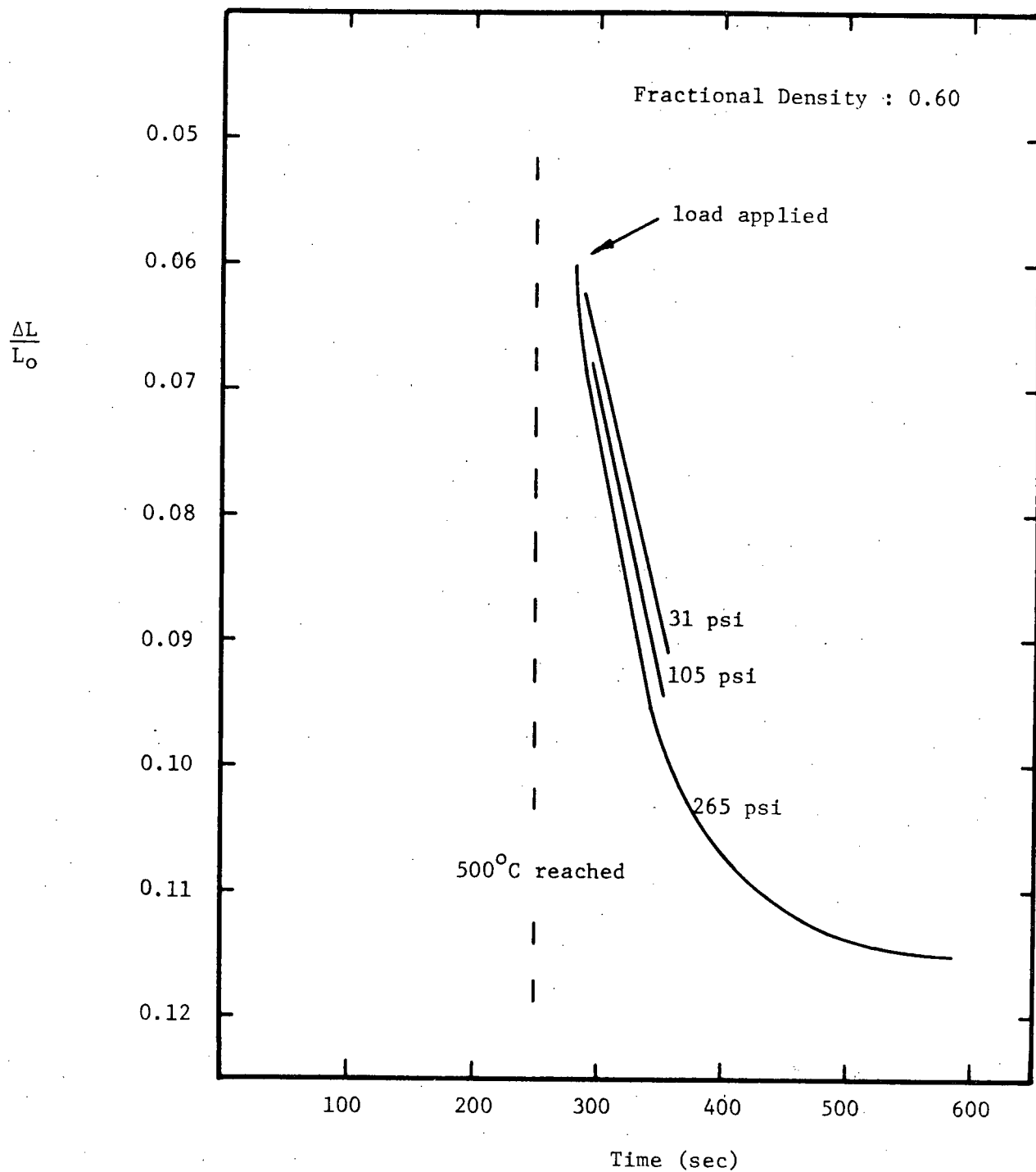


Figure 13: Stress Dependence of Creep at 550°C.

data analysis. Table I on page 33, summarizes the creep rates obtained over the temperature range 350 - 550°C and under different stresses in the range 31 to 265 psi.

## II.6 DENSITY DEPENDENCE OF CREEP

The effect of density on the creep behavior of the compacts was studied by using specimens having various fractional densities ranging from 0.42 to 0.68. For this purpose, the creep tests were carried out at 400 and 500°C under a pressure of 105 psi. Figures 14 and 15 show some of the creep curves of tests made at 400°C and 500°C. Table II shows creep rates for the complete series of specimens used to study the density dependence of creep.

## II.7 COMPLEMENTARY EXPERIMENTAL WORK

### a) Creep tests with Kaolinite

Creep tests were made at 575 and 600°C under 105 psi to study the behavior of another hydroxide mineral under identical testing conditions. The results are shown in Figure 16.

### b) Electron microscopy study

A few specimens, after the creep test, were fractured perpendicular to their cylindrical axis. Direct replicas were made by shadowing gold on the fractured surface and subsequently evaporating a layer of carbon. To detach the carbon film, the alumina specimens were dissolved in hydrochloric acid. Electron micrographs are shown in Figure 17.

### c) Weight loss vs. shrinkage

A series of specimens were heated for different periods in air

at 350°C and in vacuum (5 torrs) at 500°C in order to correlate the weight loss or fraction reacted with the creep. The results are included in Table III.

d) Measurements of specific surface areas

Samples of 1 gram of boehmite powder were heated in vacuum (5 torrs) at 500°C and in air at 400°C and 500°C for different periods. Their specific surface was measured with an Aminco Sor-BET machine. Table IV shows the values obtained.

e) Compressive strength of the compacts

In order to correlate the strength of a compact with the extent of the reaction, a series of specimens were deformed under 105 psi at 400°C and 500°C for various periods. Their strength in compression was determined in an Instron testing machine. The cross-heads displacement was 0.05 inch per minute. The results are summarized in Table V.

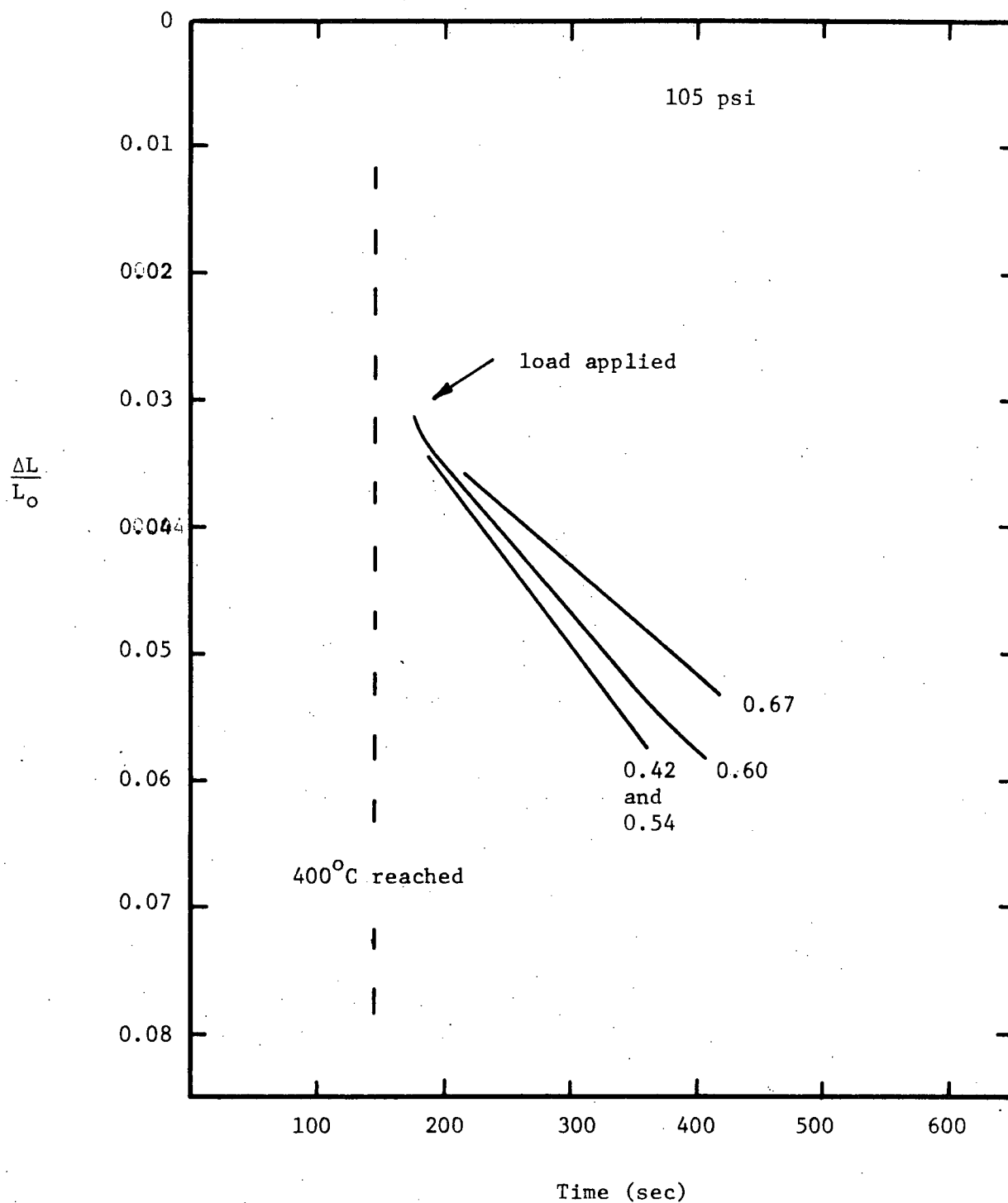


Figure 14 : Fractional Density Dependence of creep at 400°C

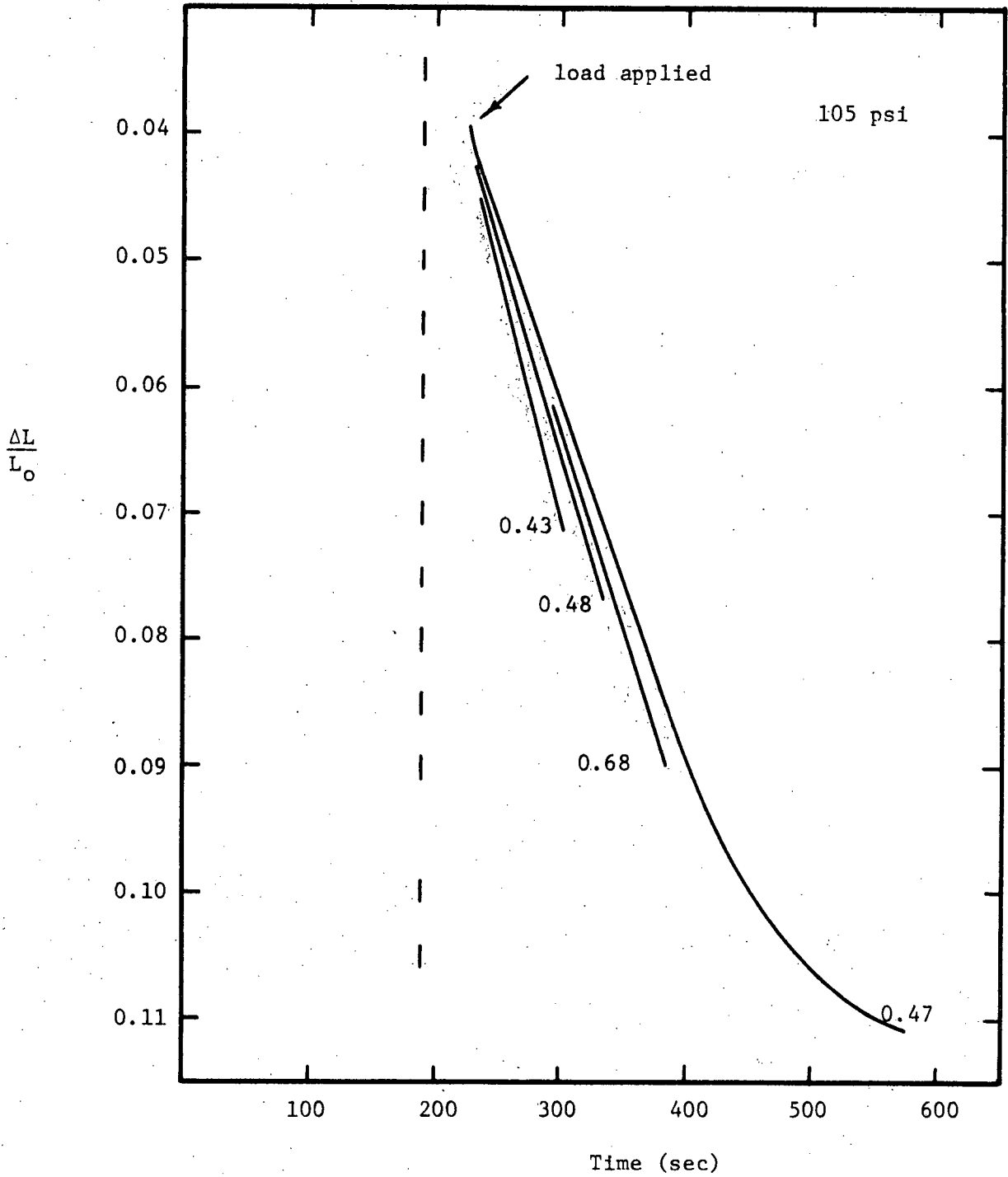


Figure 15 : Fractional Density dependence of Creep at 500°C

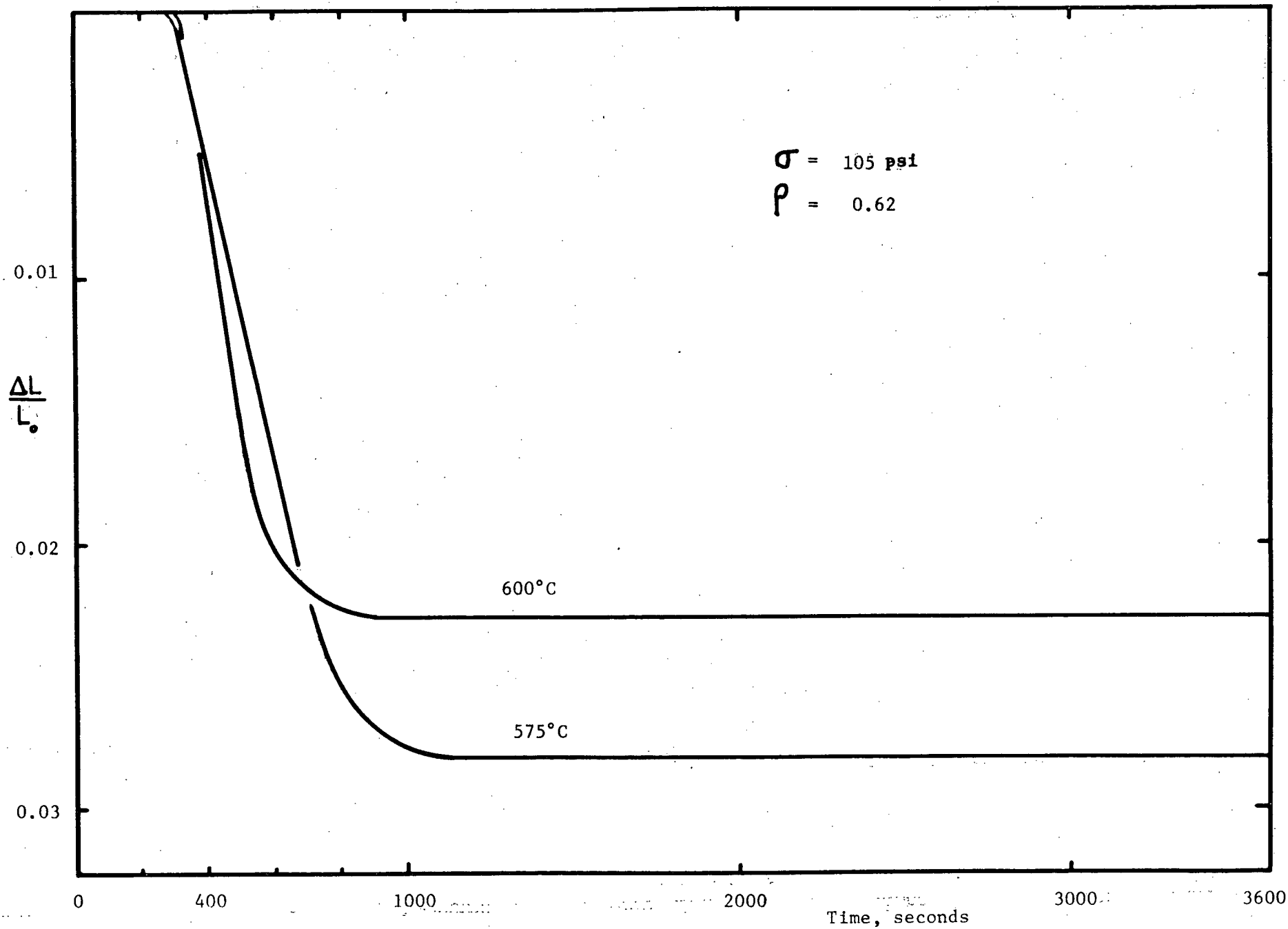
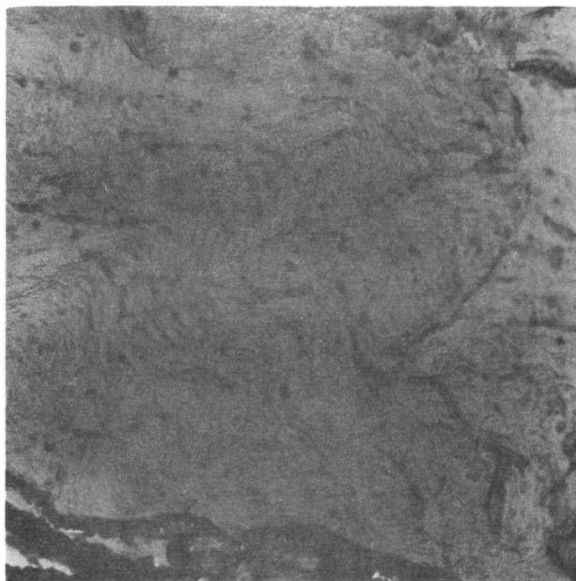
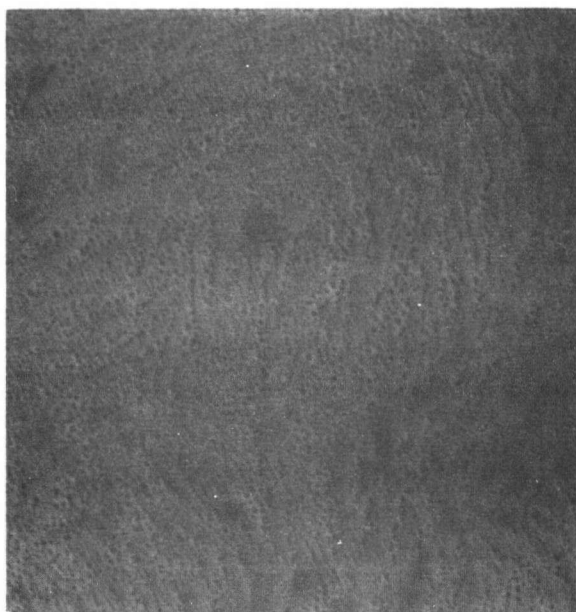


Figure 16 : Creep of Kaolinite.

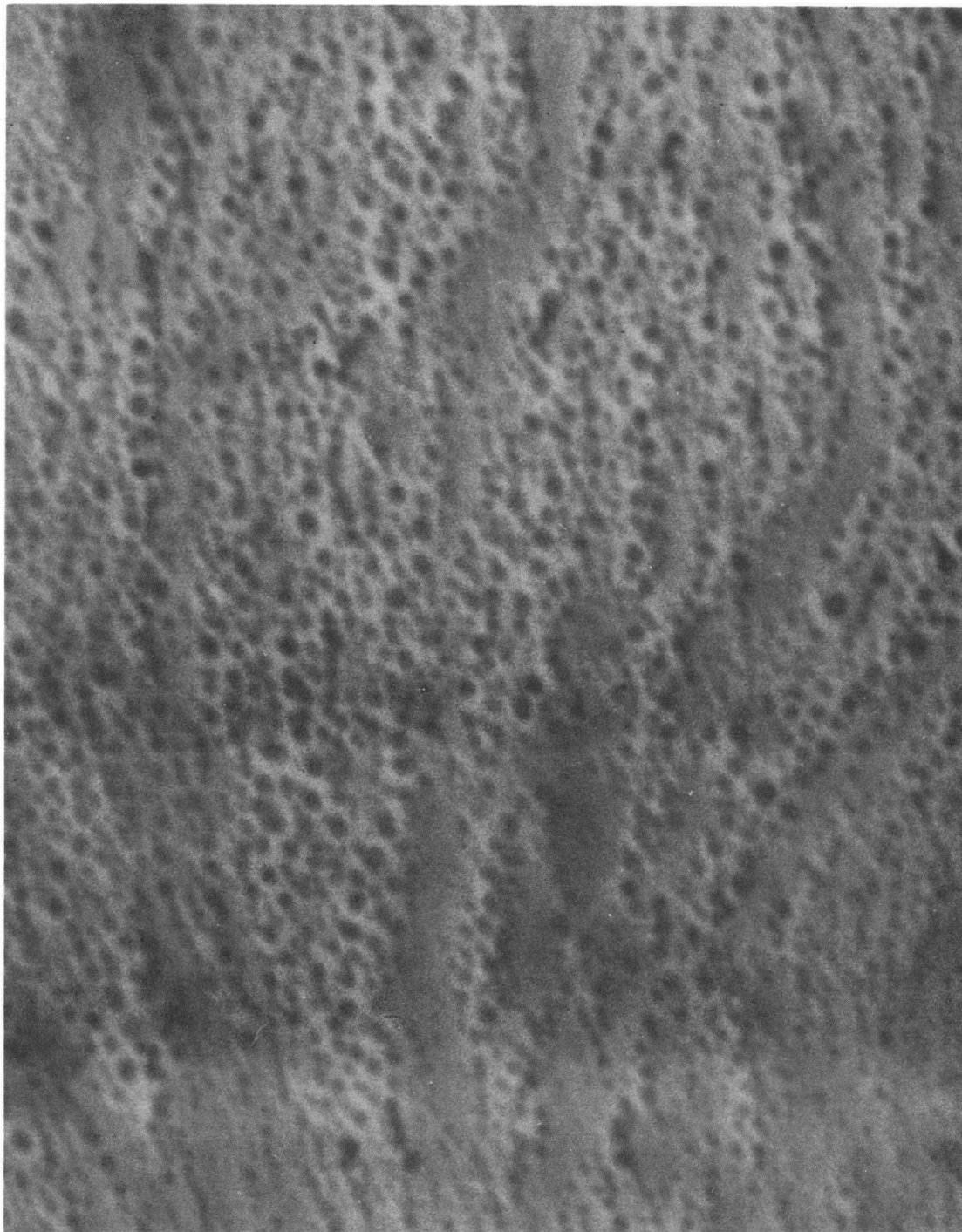


(a) X15,000



(b) X75,000

Figure 17(a) and (b) : Replica electron micrographs of fractured surface of boehmite compact after dehydroxylation.



X200,000

Figure 17(c) : Replica electron micrograph of fractured surface of boehmite compact after dehydroxylation.

TABLE I

STRESS DEPENDENCE OF THE CREEP RATE\*

	CREEP RATES $10^{-5} \text{ sec}^{-1}$				
	350°C	400	450	500	550°C
31 psi	5.7 ± 0.6	10.0 ± 1.0	18.2 ± 1.5	25 ± 2	43 ± 3
61	5.9	10.7	18.4	25	45
105	7.8	11.8	18.2	29	46
155	7.4	12.0	19.4	30	48
265	10.7	15.3	22.5	31	48

\* Fractional Density of 0.60

TABLE II

FRACTIONAL DENSITY DEPENDENCE OF THE CREEP RATE\*

CREEP RATES $10^{-5} \text{ sec}^{-1}$			
400°C		500°C	
Density		Density	
0.42	12.9 ± 1.0	0.43	35 ± 2
0.45	11.5	0.45	29
0.54	12.6	0.47	28
0.56	12.0	0.48	34
0.60	12.0	0.63	30
0.67	8.7	0.68	32

\* Applied Stress : 105 psi

TABLE III

FRACTION REACTED AS A FUNCTION OF TIME

500°C in vacuum		350°C in air	
0* min.	0.30	2 min.	0.30
½	0.60	6	0.13
1	0.70	15	0.21
2	0.93	30	0.23
5	0.96	60	0.37
60	1.00		

\* Due to Heating Period

TABLE IV

SPECIFIC SURFACE AREA\* AS A FUNCTION OF TIME

500°C in vacuum		500°C in air		400°C in air	
105 sec.	301 m <sup>2</sup> /gm	105 sec.	255 m <sup>2</sup> /gm	180 sec.	262 m <sup>2</sup> /gm
170	326				
330	309	15 min.	317		
1 hr.	319				
2½ hr.	283	18 hrs.	270	12 hrs.	288 m <sup>2</sup> /gm

\* ± 10%

TABLE V  
COMPRESSIVE STRENGTH OF SPECIMENS  
AFTER DEHYDROXYLATION

400°C		500°C	
50 sec	990 psi	40 sec	1600 psi
80	1100	50	1750
100	1400	70	2200
150	1350	80	1950
200	1700	120	2250
300	1650	150	2900

### III. DISCUSSION

#### III.1 EFFECT OF THE SOAKING TIME

The compacts have been found to shrink even before the application of the load (Figure 9). If the soaking time is extended from 30 to 210 seconds this shrinkage increases from 4 to 6.5% as shown by the typical curves of Figure 18. As the testing conditions were identical with respect to temperature ( $500^{\circ}\text{C}$ ) and stress (265 psi), the creep curves are parallel as expected. When the load was applied after a long soaking period, the reaction was partially completed, so that the contribution of the applied stress to the overall creep was short and the total creep was correspondingly smaller than when the load was applied without any soaking period.

In order to establish a relation between the shrinkage observed during the dehydroxylation reaction and the creep itself, experiments were carried out in which the weight loss of the specimen was determined under the same heating conditions as were used for the creep study. The variation of specific surface area of boehmite on calcination was also determined. This is important as it has been shown<sup>(13)</sup> that for most hydroxides, surface area increases considerably after calcination. Figure 19 shows the results of three different experiments; creep, fraction decomposed and surface area at  $500^{\circ}\text{C}$ . as a function of time. The creep experiment was made under 265 psi. A series of powder samples have been heated in vacuum at  $500^{\circ}\text{C}$  for different periods. The fraction reacted was calculated from the weight loss measurements. The curves

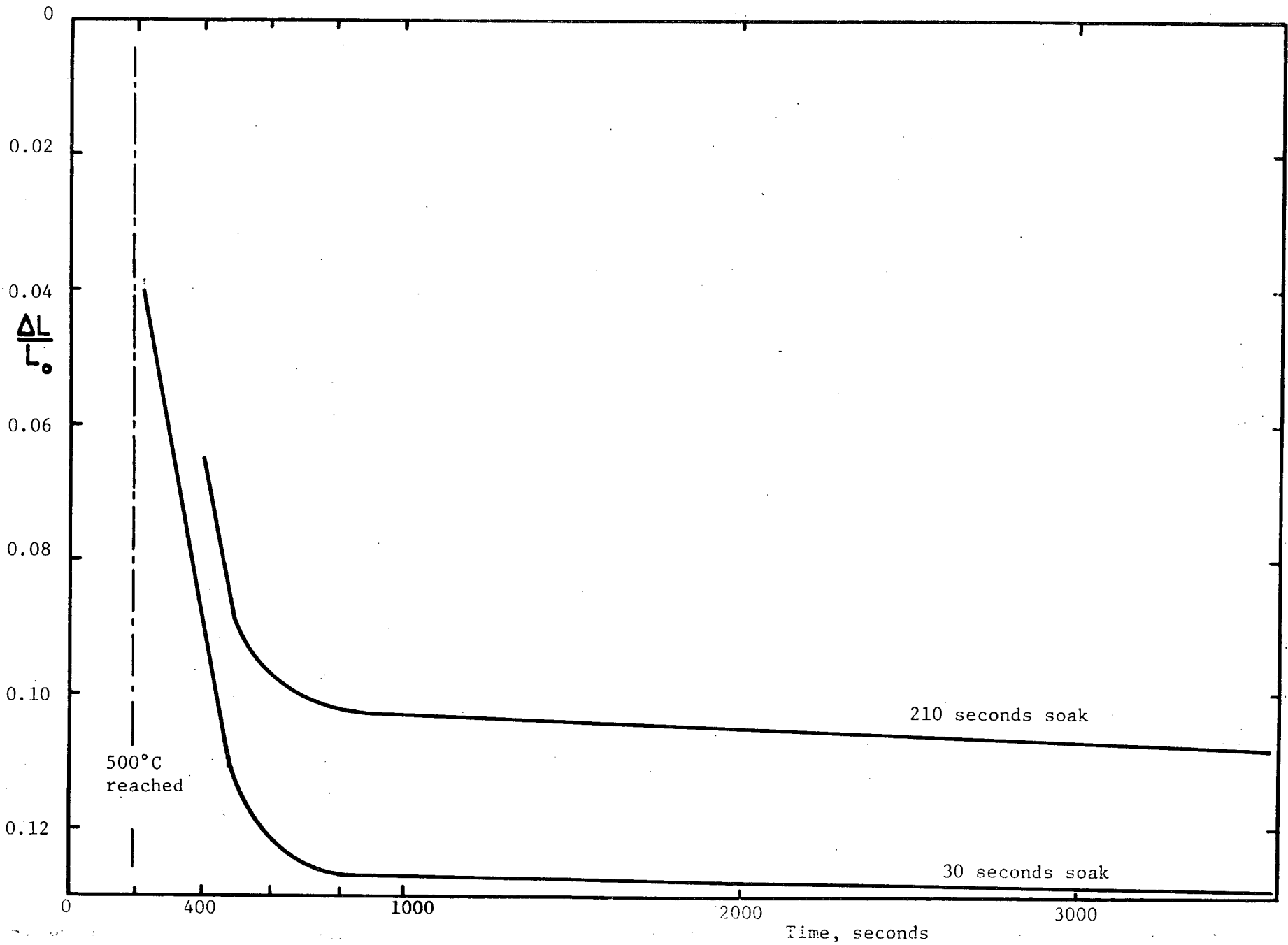


Figure 18: Creep at 500°C, under 265 psi and after different soaking times.

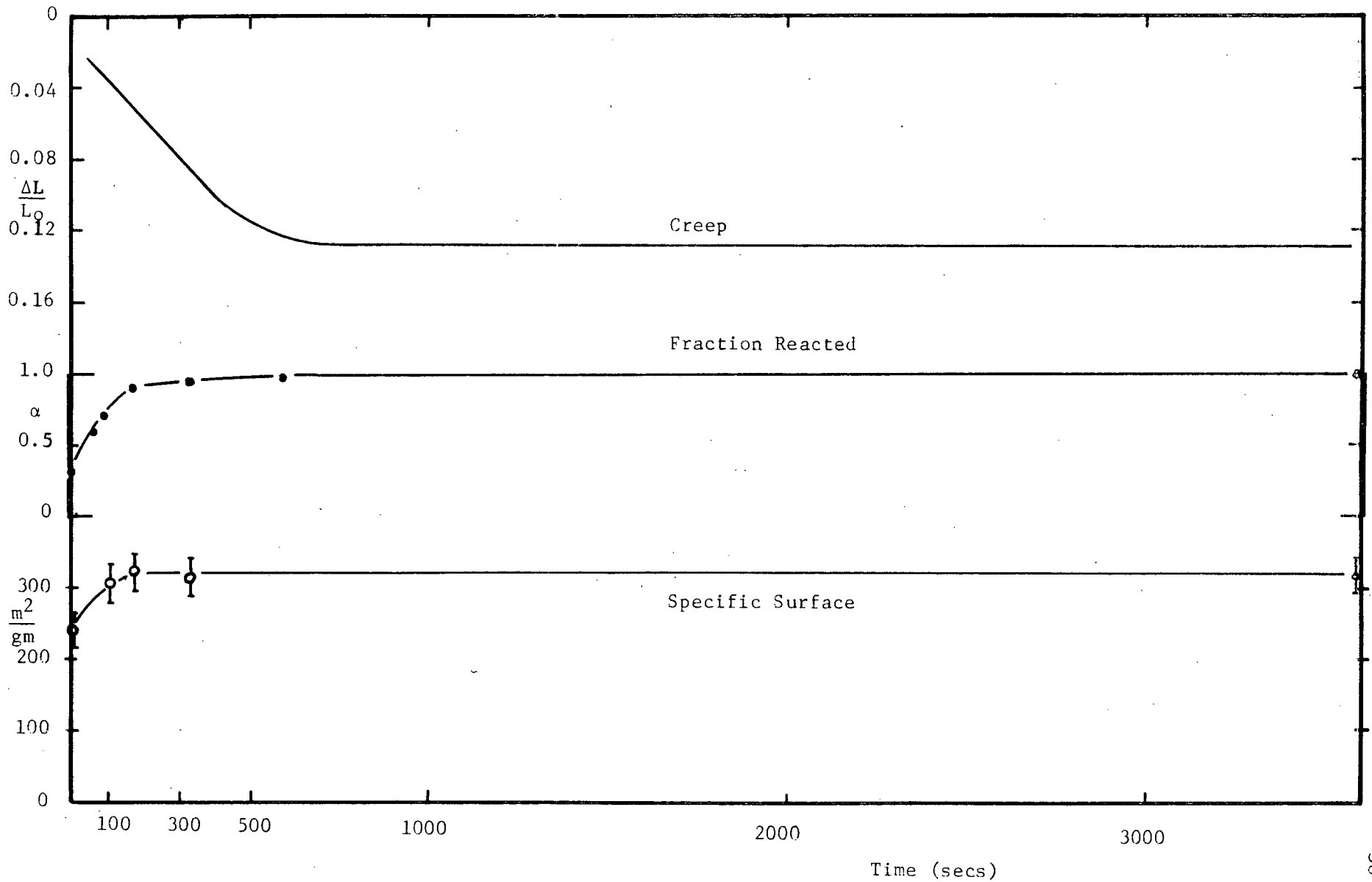


Figure 19 : Creep, fraction decomposed and surface area as a function of time at 500°C

for the specific surface area and the fraction reacted reached steady values in a shorter time than the creep curve. This difference can be explained as being due to the fact that removal of the vapour phase is faster from a loose powder such as used for the surface area and the percentage transformed test than from a compact as used for the creep measurements. The presence of water vapor pressure in the compact may also have reduced the rate of the reaction<sup>(14)</sup>. Hence, it appears reasonable to say that the creep deformation ceases when the reaction is over. The small increase in surface area (250 to 320 m<sup>2</sup>/gm) has been explained by Iler<sup>(11)</sup> as due to increase in internal porosity.

A dispersed sample of the boehmite powder was heated on a carbon film in the hot-stage of the Hitachi electron microscope. The specimen was not exposed to the electron beam except to take photographs at different temperatures. Up to 800°C, no significant change of the specimen was observed. However, at 50,000 magnification, the resolution of the thin ceramic fibers was very poor.

### III.2 CREEP DUE TO SURFACE TENSION

The creep behavior of boehmite during the dehydroxylation reaction is very different from the creep behavior of kaolinite and magnesium hydroxide. With no applied stress it has been observed that a compact of kaolinite undergoes a change in linear dimension of less than 0.5% during its dehydroxylation reaction although it incurs a weight loss of 14%. Figure 16 shows two creep curves of kaolinite. When the specimen was maintained for 30 seconds at 575 or 600°C (before the load was applied) the dimensional change of

the compact was negligible. In the case of magnesium hydroxide, Sunderland<sup>(13)</sup> reported 0.5% shrinkage under zero load compared to a total creep of 8% at 400°C and under 210 psi. This shrinkage in the case of boehmite may be up to 10% (Figure 10).

Before any shrinkage can take place interaction between points of contact is necessary. The free energy change that gives rise to shrinkage of a powder compact is the decrease in surface area and lowering of the surface free energy by the elimination of solid-vapor interface. The driving force for neck-growth between two particles is the effective stress associated with the radius of curvature at the points of contact. This stress is inversely proportional to the radius of curvature. The fibers of the boehmite powder studied have a diameter of about 0.005 $\mu$ . Using the general formula  $\frac{2\gamma}{R}$ , where  $\gamma$  is the surface energy and R is the radius of curvature and assuming a surface energy as low as 100 ergs per cm<sup>2</sup>, the stress at the point of contact between two fibers of boehmite is over 10,000 psi. This stress is much larger than those applied in the creep study and is expected to induce the necks (points of contact) between the particles to grow.

### III.3 NECK FORMATION

In order to see if there was any evidence of neck formation, compacts were fractured perpendicularly to the cylindrical axis. Direct replicas were made on the fractured surfaces and examined in the electron microscope. Figure 17(a) shows that the texture is composed of bent but aligned fibers. It appears that the fibers were aligned in parallel arrays during the cold compaction of the powder (Figure 4(a)).

During the dehydroxylation reaction, a great number of necks were formed between adjacent fibers in order to lower the stress associated with the small radius of curvature at the points of contact. Figures 17(b) and 17(c) show the fractured surface at higher magnifications. The black spots which are aligned are voids between two adjacent fibers, fused at the points of contact. Between two parallel rows of black spots the fibers are discernable. The material transport associated with the neck growth has created these voids and also produced the shrinkage of the compact, which in turn produced the creep observed during the experiments.

#### III.4 EFFECT OF THE DENSITY ON THE CREEP RATE

The creep rate as a function of the green density is shown in Figure 20. It is apparent from the figure that creep rate is almost independent of the density, although this cannot be conclusive because of the scatter of the data, particularly with the low-density specimens. This may be due to the fact that the fibers are aligned (Figure 17(a)) and that the total number of points of contact between them do not change very much by varying the density.

#### III.5 PARTICLE DEFORMATION

The neck formation observed in the case of the creep of boehmite compacts during dehydroxylation cannot by itself explain the fact that it is possible to obtain a body of theoretical density under reactive hot-pressing conditions. In effect, if sufficient pressure is applied in a closed die, the pores can eventually be eliminated and specimens of the theoretical density produced.

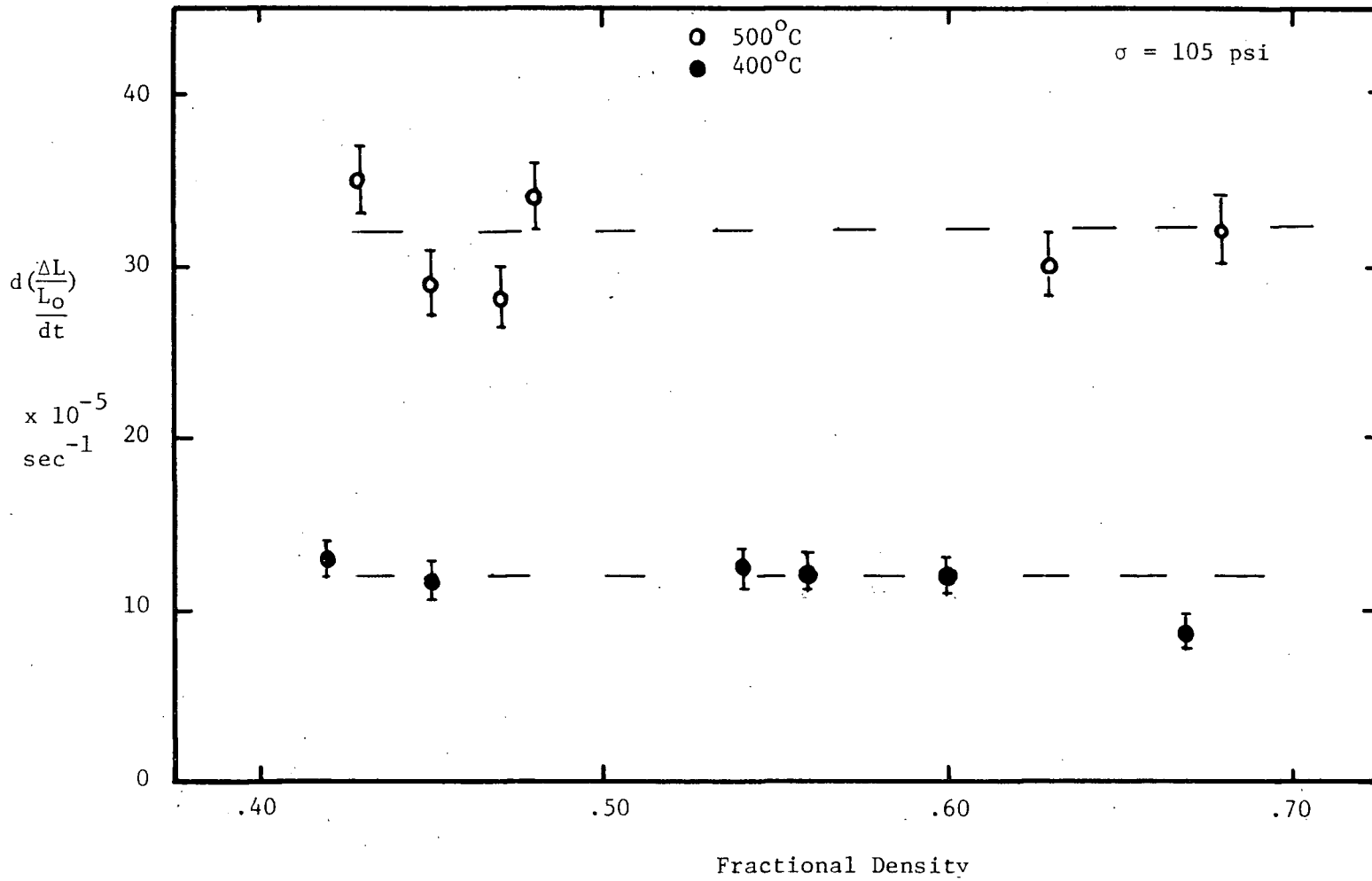


Figure 20 : Creep Rate as a Function of Fractional Density.

The driving force for the growth of the necks is the small radius of curvature associated with the neck. At the same time, the theory predicts that the driving force decreases as the size of the neck increases and that this leads to an end-point density which is different from the true density. By applying a stress as low as 265 psi in the creep experiments, the creep rate was increased from 10 to 50 % depending on the test temperature, whereas the total creep was increased from 50 to 100 %. Hence, it is believed that the applied stress caused some particle deformation during the dehydroxylation reaction.

### III.6 PHENOMENOLOGICAL EQUATION OF THE CREEP RATE

The creep rates between 350 and 550°C under 31 to 265 psi with compacts having a fractional density of 0.6 are shown in Table I page 33. These creep rates  $\dot{\epsilon}_T$  are plotted as a function of the applied stress as shown in Figure 21. It can be seen that the creep rate is proportional to the applied stress at a constant temperature at least in the range of stresses studied. By extrapolating the curves on Figure 21 to zero stress a creep rate  $\dot{\epsilon}_0$  is found for each temperature.

If  $\dot{\epsilon}_0$  is subtracted from  $\dot{\epsilon}_T$ , a value  $\dot{\epsilon}_S$  is obtained.

$$\dot{\epsilon}_S = \dot{\epsilon}_T - \dot{\epsilon}_0$$

This value  $\dot{\epsilon}_S$  is the creep rate caused by the applied stress.  $\log \dot{\epsilon}_S$  is plotted as a function of  $\log \sigma$  (applied stress) in Figure 22. In spite of the experimental scatter, the best line that can be drawn has a slope

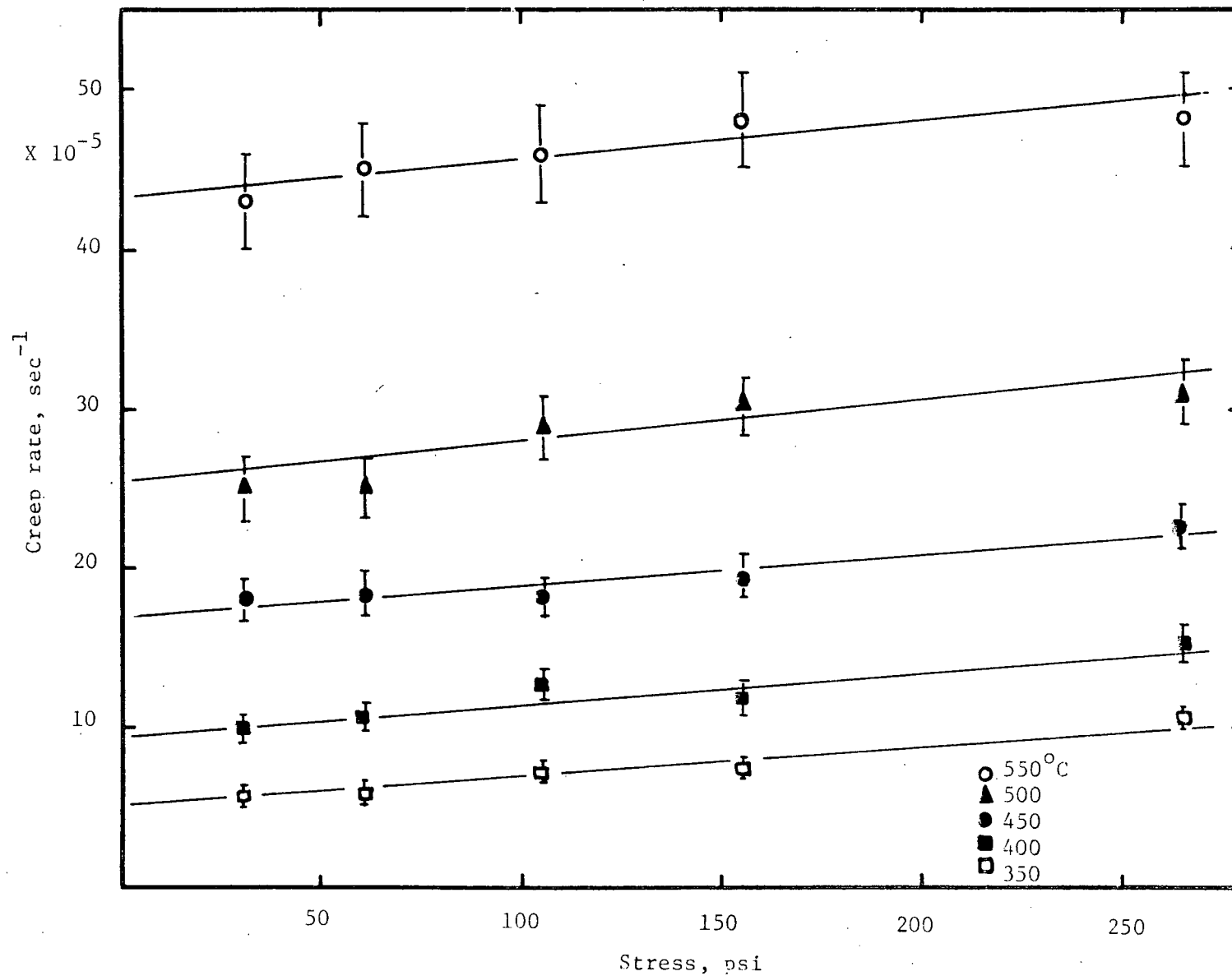


Figure 21 : Creep rate vs. stress at different temperatures.

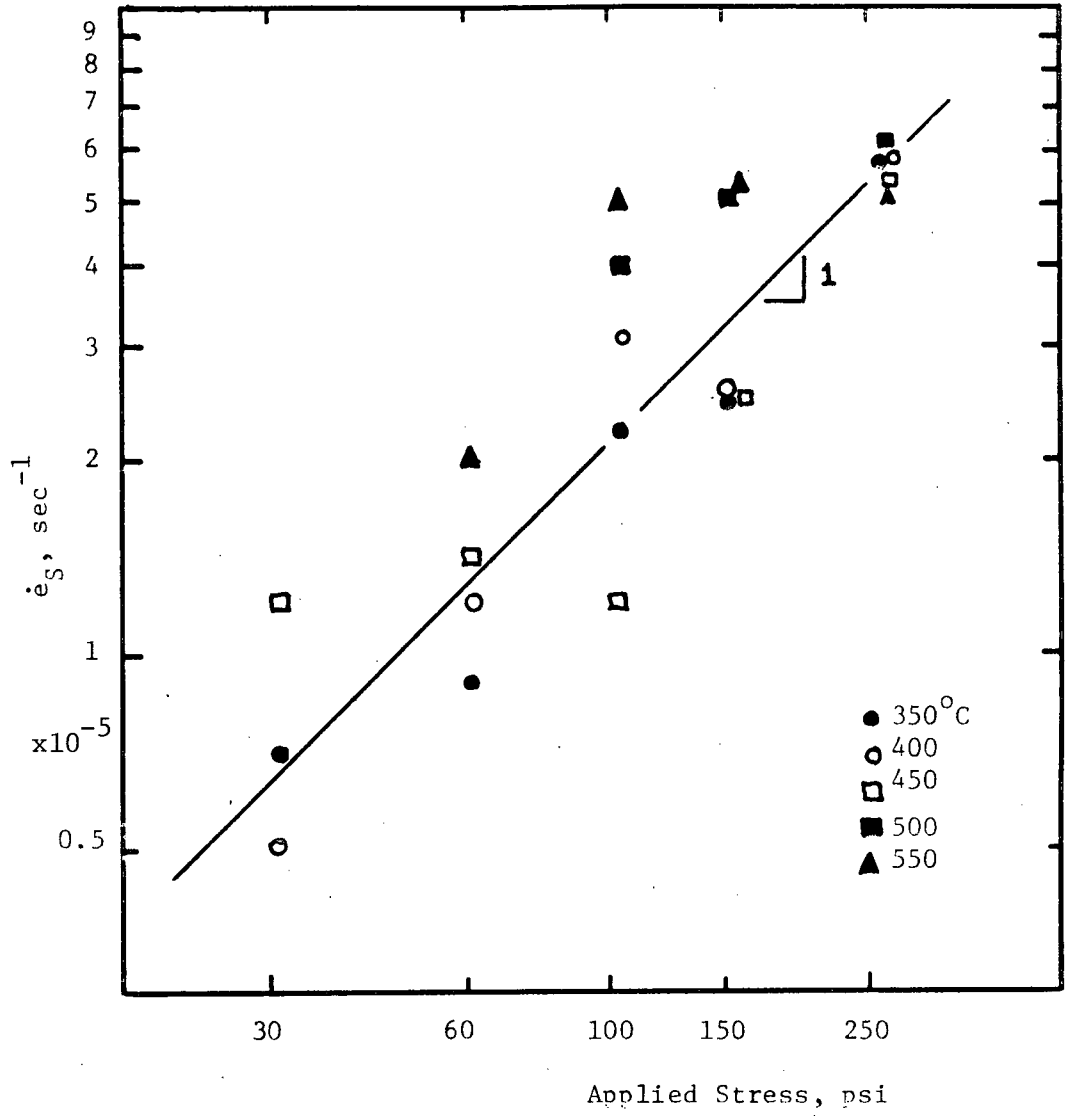


Figure 22 :  $\log \dot{\epsilon}_S$  vs.  $\log \sigma$ .

of one. This indicates a direct proportionality between the creep rate and stress. This behavior is usually attributed to viscous flow, grain boundary sliding and Nabarro-Herring creep. The following sections give further information about the possible mechanism.

The fact that the points corresponding to different temperatures are scattered randomly on both sides of the line, indicates that the creep rate due to the stress only is temperature independent.

The values  $\dot{\epsilon}_0$  indicate that deformation occurred even when no external stress was present. This creep or shrinkage has been verified experimentally at 500°C (Figure 10) and was found to be  $21 \times 10^{-5} \pm 2 \text{ sec}^{-1}$  which is slightly lower than that of the extrapolated value of  $25 \times 10^{-5} \text{ sec}^{-1}$ .

Hence the phenomenological equation has two terms:

$$\text{Creep rate} = \dot{\epsilon}_0 + b\sigma^{n=1} \quad (1)$$

The term  $\dot{\epsilon}_0$  is the contribution of the surface tension to the total creep. The term "b" is the coefficient of the applied stress.

Figure 23 shows the log of the creep rate as a function of the reciprocal of the absolute temperature of the test (an Arrhenius plot). The shrinkage rates given by the extrapolation at  $\sigma = 0$  are also included in the plot. The activation energy has been calculated from this plot and found to be  $9.1 \pm 1.5 \text{ Kcal/mole}$ . The phenomenological equation (1) therefore becomes:

$$\text{Creep rate} = A \exp\left(\frac{-9,100 \pm 1,500}{RT}\right) + B\sigma$$

with the values of the parameters A and B given in Table VI. "A" is calculated from the extrapolated values at  $\sigma = 0$ , "B" is calculated from the creep data at 265 psi.

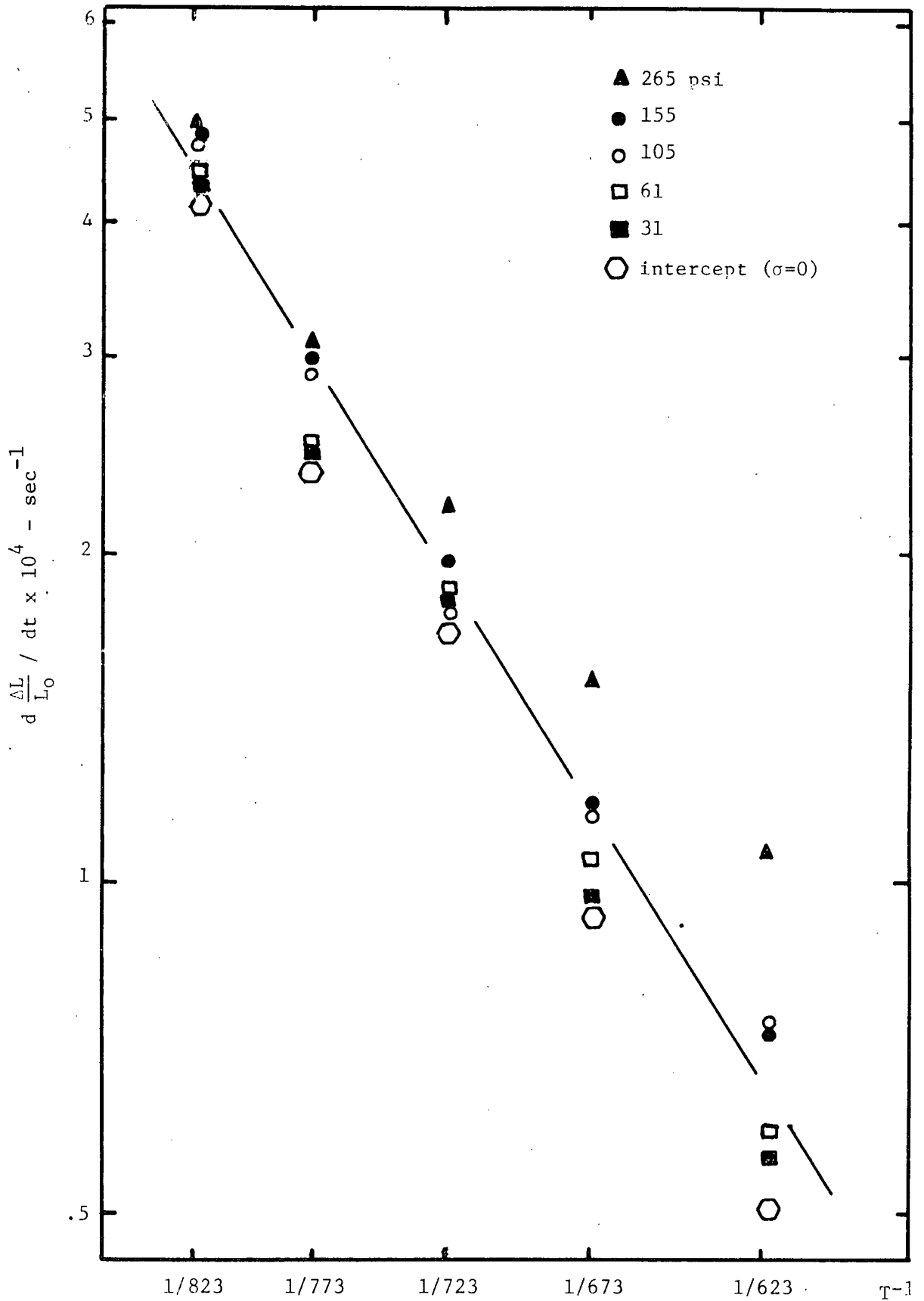


Figure 23 : Log of creep rates as a function of the reciprocal of the absolute temperature.

TABLE VICOEFFICIENTS OF THE EQUATION

$$\text{Creep rate} = A e^{-\frac{9,100}{RT}} + B\sigma$$

at 60% Density

Temperature	A sec <sup>-1</sup> Surface Energy	B sec <sup>-1</sup> psi <sup>-1</sup> Applied Stress
350°C	0.130	1.9 x 10 <sup>-7</sup>
400	0.136	1.9 x 10 <sup>-7</sup>
450	0.146	1.9 x 10 <sup>-7</sup>
500	0.140	2.6 x 10 <sup>-7</sup>
550	0.164	2.6 x 10 <sup>-7</sup>
Average	0.144	2.2 x 10 <sup>-7</sup>

The final form of the equation is:

$$\text{Creep rate} : \left[ 0.144 \exp \left( \frac{-9,100 \pm 1,500}{RT} \right) + 2.2 \times 10^{-7} \sigma \right] \text{ sec}^{-1}$$

The kinetic study of the decomposition of boehmite (300 to 400 $\mu$ ) by Callister et al<sup>(14)</sup> has produced an activation energy of 67 - 70 Kcal/mole which is essentially independent of the water vapor partial pressure ranging from 0.00 (dry nitrogen) to 0.50 atm. Eyraud and Goton<sup>(15)</sup> calculated an activation energy of 42 Kcal/mole at a pressure of 1 torr similar to the pressure at which the experiments of this study were made. Callister explained the discrepancies (42 compared to 70 Kcal) by the possibility of a different mechanism being responsible for the reaction in a vacuum.

Compared to 42 Kcal/mole, the activation energy for creep found in this study (10 Kcal/mole) is considerably smaller. This is also the case for magnesium hydroxide, where the activation energy for creep is 17 Kcal/mole<sup>(13)</sup> compared to 29-43<sup>(16)</sup> for the dehydroxylation reaction. In the case of kaolinite, the creep curves shown in Figure 18 give an activation energy of about 15 Kcal for the creep compared to 38 - 65<sup>(17)</sup> for the dehydroxylation reaction. From this general observation it is concluded that the creep is not controlled by the dehydroxylation reaction. However, as the material does not creep before the start of the dehydroxylation reaction, it is reasonable to assume that the creep process was initiated by the dehydroxylation reaction.

It is believed that the very small size of the fibers may be an important factor in the kinetics of creep. The neck formation

between the fibers suggests that the creep activation energy may be related to the activation energy for neck growth between alumina crystals. The only data available are for large alumina spheres ( $>1\mu$ ). At high temperatures (1600 - 1900°C) the activation energy for neck growth is 140 - 150 Kcal<sup>(18)</sup>. The activation energy for surface diffusion of  $Al_2O_3$  has been reported<sup>(19)</sup> to be 75 Kcal/mole.

However, the boehmite fibers used in this study can be compared to polymeric chains and it is interesting to note that the activation energy for creep of polymers above the glass transition temperature is close to the activation energy for polymerisation. The activation energy for diffusion of a small molecule in a polymer lies between 5 and 15 Kcal/mole °C<sup>(20)</sup> and the activation energy for polymerisation of butadiene<sup>(21)</sup> in the presence of cobalt is 12.7 Kcal/mole. This suggests that there may be similarities between the creep of fibrillar boehmite and the flow behavior of organic polymers. Studies of the very early stages of grain growth of alumina may well help to elucidate the rate controlling mechanism of the creep process observed in this investigation.

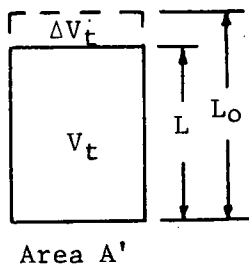
### III.7 EQUATION RELATING THE CHANGE OF LENGTH OF THE COMPACTS WITH TIME

A theoretical equation has been developed by Wadsworth and Chaklader<sup>(22)</sup>, for the densification process during a dehydroxylation reaction. The main considerations in this theoretical development are

- a) that the particles are spherical in shape,
- b) they deform at the points of contact under axial pressure in a die and the cross-sectional area of the specimen remains constant during compaction.

In the present investigation, the specimens were tested under creep conditions and not under hot-pressing conditions as postulated in the theory. However, it has been observed experimentally that the diametral shrinkage due to the dehydroxylation reaction was almost compensated by the bulging due to the compressive stress and as a consequence the change in the diameter of the compact after the creep was less than 0.5%. This behavior may be considered equivalent to the change of linear dimension in a compacting die where there is no diametral shrinkage.

The essential steps in the derivation are included here, as this has not yet been published. For a double acting die of constant cross-sectional area  $A'$ , at time  $t = 0$  the total number of particles is  $n_0 A' L_0$ , where  $n_0$  is the number of particles per unit volume and  $L_0$  is the initial specimen length. After deformation at time  $t$ , this



will be  $nA'L$  where  $n$  is the total number of particles per unit volume after deformation and  $L$  is the new length. Hence,

$$n_0 L_0 A' = n L A' \quad (1)$$

The number of particles per unit volume ( $n$  or  $n_0$ ) will depend on the packing geometry which includes the co-ordination number and location of the nearest neighbours. Then  $n_0$  can be defined as  $1/(4/3\pi r_0^3) p_0$ , where  $p_0$  is the packing factor, and  $r$  is the average particle radius. This relation can be rewritten as

$$n_0^{1/3} = \frac{K p_0^{1/3}}{r_0} \quad (2)$$

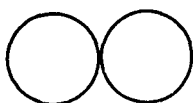
and after deformation

$$n^{1/3} = \frac{K p^{1/3}}{r} \quad (3)$$

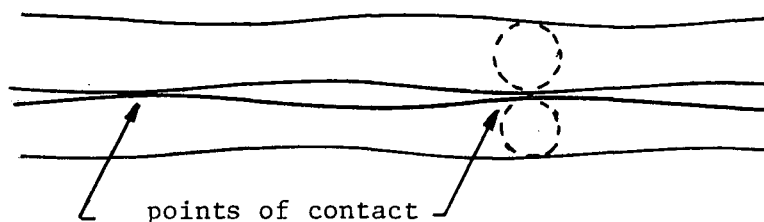
Assuming that the same packing geometry is being retained, while the reaction proceeds, i.e.  $p \approx p_0$  and introducing equations (2) and (3) into (1), we obtain

$$\frac{L}{r^3} = \frac{L_0}{r_0^3} \quad (4)$$

In the case of fibers the material can be assumed to behave similarly to spheres. A cross-section of two parallel fibers indicates that in two dimensions the situation is identical to the case of spheres:



In the third dimension, if points of contact are assumed, then the geometry of neck growth between fibers will also be similar to the neck growth between spheres at the points of contact. This has been shown by Kuckzynski<sup>(22)</sup> and is illustrated schematically in the following figure:



Considering a single particle where  $V_S$  is the volume of the spherical particle and  $V_{S0}$  is the original volume

$$V_S = \frac{4}{3}\pi r^3$$

$$\Delta V_S = 4\pi r^2 \Delta r$$

$$\frac{\Delta V_S}{V_{S_0}} = \frac{3r^2 \Delta r}{r_0^3} = 3 \left(\frac{r}{r_0}\right)^2 \left(\frac{r_0 - r}{r_0}\right) \quad (5)$$

$V_S$  can also be expressed by

$V_S = \frac{Z}{2} V_n$  where  $Z$  is the co-ordination number and  $V_n$  is the volume of a neck. For most of the mass transport mechanisms (volume, surface . . .)

$$V_n = \frac{\pi x^4}{2r} \text{ where } x \text{ is the neck radius.}$$

$$\Delta V_S = \frac{Z \pi x^4}{4r} \quad (6)$$

Combining equations (6) and (5)

$$\frac{\Delta V_S}{V_{S_0}} = 3 \left(\frac{r}{r_0}\right)^2 \left(\frac{r_0 - r}{r_0}\right) = \frac{Z \pi x^4}{4r [4/3 \pi r_0^3]} \quad (7)$$

$$\left(\frac{r}{r_0}\right)^3 \left(1 - \frac{r}{r_0}\right) = \frac{Z x^4}{16 r_0^4} \quad (8)$$

In sintering theory, the neck radius is related to time by the following relationship

$$x = K t^{1/n} \quad (9)$$

where "n" is an integer whose value depends on the mechanism of mass transport:

- 2 - viscous flow
- 3 - evaporation condensation
- 5 - volume diffusion
- 6 - grain boundary diffusion
- 7 - surface diffusion

Equation (8) becomes

$$\left(\frac{r}{r_0}\right)^3 \left(1 - \frac{r}{r_0}\right) = \frac{K'}{r_0^4} t^{4/n} \quad (10)$$

Using equation (4) the final form of the equation for shrinkage becomes

$$\frac{L}{L_0} \left[1 - \left(\frac{L}{L_0}\right)^{1/3}\right] = K'' t^{4/n} \quad (11)$$

Typical creep data obtained in this investigation have been used to verify equation (11). In order to determine the operating model,  $\log \left\{ \frac{L}{L_0} \left[ 1 - \left( \frac{L}{L_0} \right)^{1/3} \right] \right\}$  has been plotted against log time. The linear portion of the creep curves have been extrapolated to  $\frac{\Delta L}{L_0} = 0$  in order to find a time,  $t = 0$ , corresponding to the beginning of the neck formation at the test temperature.

Figure 24 shows the plot of the shrinkage data obtained at different temperatures (350, 400, 500 and 550°C) under 265 psi and with compacts of 0.60 fractional density. It appears that over a certain period the theoretically predicted relationship between the shrinkage and time is obeyed. After a longer period, however, the data tend to deviate from the prediction. The slope  $(4/n)$  in the linear region varies between 0.80 and 0.90 which indicates that "n" is approximately equal to 5. According to Kuczynski's derivation, when n is equal to 5 the neck growth and shrinkage is controlled by volume diffusion. However, it should be pointed out that although from this analysis an indication about the nature of the mechanism involved in the creep process can be obtained, no conclusion should be drawn without much extensive work.

### III.8 STRENGTH OF THE COMPACTS AS A FUNCTION OF TIME

From the discussion of the preceding section (III.7) it is expected that with the formation of necks at the points of contact, the compacts will acquire some strength, which will increase with the growth of the neck. With these assumptions, an equation relating the strength as a function of time has been derived<sup>(22)</sup> and given below.

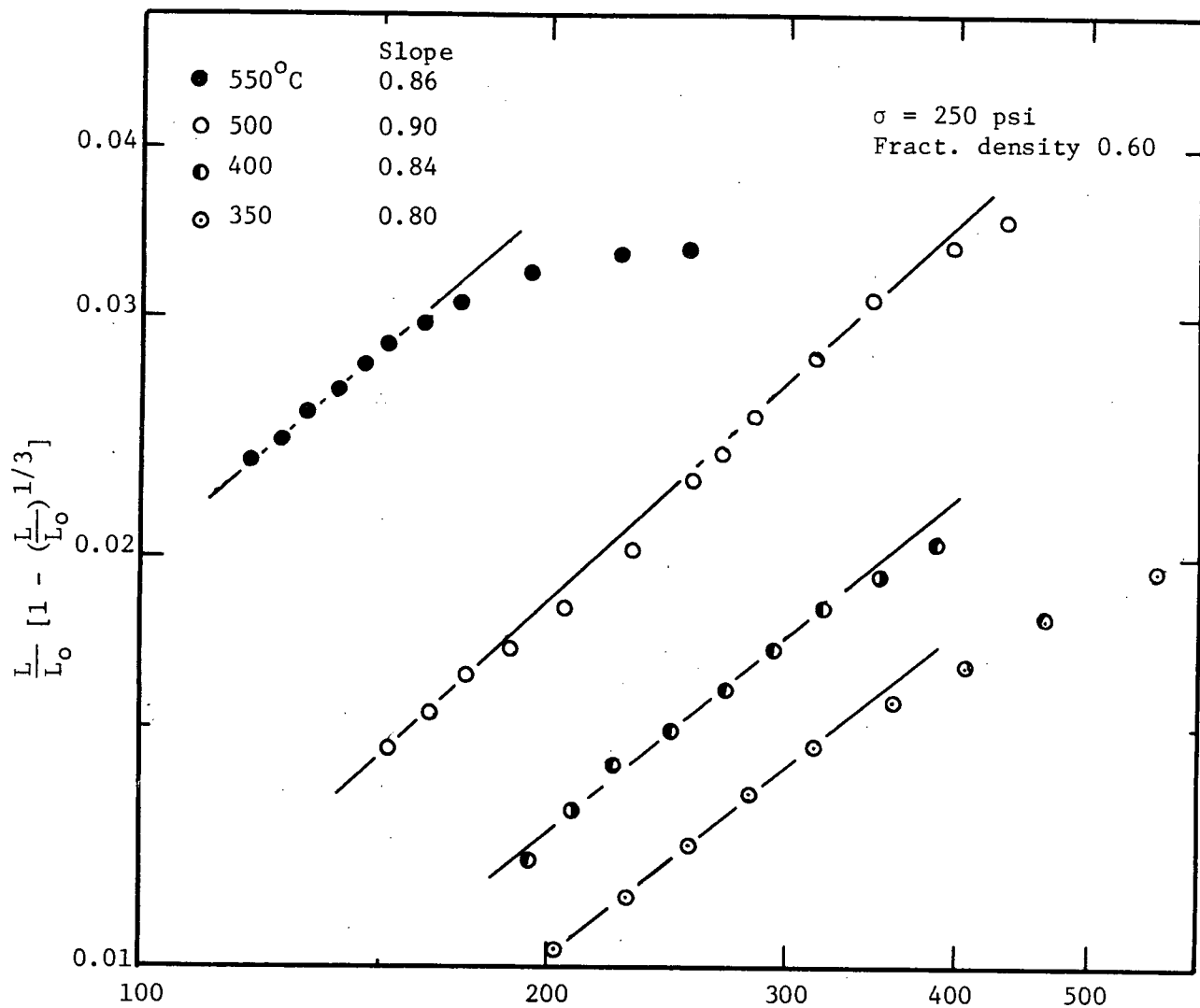


Figure 24 :  $\text{Log } \frac{L}{L_0} [1 - (\frac{L}{L_0})^{1/3}]$  vs.  $\text{log } t$

The strength  $S$  of a compact is proportional to the strength of the necks formed between particles located on the plane where the maximum stress is acting. If we assume that the strength of a neck is proportional to its cross-section, then the strength of the compact is

$$S = K(n)^{2/3} a_p \quad (1)$$

where  $n$  is the number of particles per unit volume and  $a_p$  is the neck cross-section per particle. Due to the complexity of the mass transport (shrinkage and creep), a constant number of particles per unit volume is assumed. Moreover, it is assumed that the second stage of sintering is not reached, i.e. the number of necks is constant.

The neck cross-section per particle

$$a_p = \frac{Z}{2} a_n \quad (2)$$

where  $Z$  is the co-ordination number and  $a_n$  is the individual neck cross-section

$$a_n = \pi x^2 \quad (3)$$

where  $x$  is the neck radius. In most sintering models, the neck volume is given by

$$V_n = \frac{\pi x^4}{2r} \quad (4)$$

where  $r$  is the particle radius. From equation (3)

$$V_n = \frac{a_n^2}{2\pi r} \quad (5)$$

From the preceding section (III.7)

$$n^{1/3} = \frac{p}{2r} \quad (6)$$

where  $p$  is a packing factor.

Hence equation(5) becomes

$$V_n = \frac{a_n^2 (n)^{1/3}}{\pi p} \quad (7)$$

The unit variation of the volume of a compact due to neck formation is  $\Delta V$

$$\Delta V = \left[ \frac{Z}{2} n \right] \frac{a^2 n^{1/3}}{\pi p}$$

or

$$\Delta V = \frac{Z}{2} \frac{n^{4/3}}{\pi p} \left[ \frac{2 a^2}{Z} p \right] \quad (8)$$

Combining equations (8) and (2)

$$\Delta V = \frac{2}{\pi Z p} n^{4/3} a^2 p \quad (9)$$

Equation (1) becomes, after introducing equation (9)

$$S = K \left( \frac{\pi Z p}{2} \right)^{1/2} (\Delta V)^{1/2} \quad (10)$$

It is assumed that the mass transport mechanism is volume diffusion as has been observed in the preceding section (III.7). From Kuczynski's volume diffusion model for sintering<sup>(23)</sup>, it is simple to derive an equation of  $\frac{\Delta L}{L_0}$  as a function of time for a given temperature.

$$\frac{\Delta L}{L_0} = \frac{\Delta V}{3V_0} = K' \left( \frac{2\gamma}{r} \right)^{4/5} t^{4/5} \quad (11)$$

where  $\gamma$  is the surface energy.

For hot-pressing,  $\frac{2\gamma}{r}$  is replaced by  $\left( \frac{2\gamma}{r} + \sigma \right)$ ,  $\sigma$  being the applied stress during the dehydroxylation. Substituting  $\Delta V$  in equation (10) and regrouping the constant terms, gives

$$S = K'' \left( \frac{2\gamma}{r} + \sigma \right)^{2/5} t^{2/5} \quad (12)$$

In order to verify equation (12) a constant stress of 105 psi was used in creep experiments at 400 and 500°C for various periods. The compressive strength of the cylindrical specimens was determined in an Instron machine.

It has been noted that hydroxide compacts (magnesium hydroxide, and kaolinite, boehmite), left for a long period at a temperature immediately below the dehydroxylation range have almost no strength at all. This

drop in strength may be caused by the removal of physically adsorbed water and other volatile materials which were responsible for bonding in the green compact. From this observation it is assumed that the strength of the compacts after the dehydroxylation is caused only by the necks. The log of the strength obtained in the compression test is plotted as a function of log time in Figure 25.

$$\text{Log } S = K''' + n \log t$$

The values of  $n$  obtained (0.35 and 0.40) are in good agreement with the exponent of  $t$  (2/5) in equation (12). This indicates again that the mechanism involved in the creep process may be volume diffusion.

However, the activation energy for creep has been calculated to be only 10 Kcal/mole. This discrepancy between the usually large activation energy for volume diffusion and the small value found for the activation energy of the creep may be resolved by considering the nature of solids after the dehydroxylation reaction. In this case, the decomposition reaction produced both very fine particles (41 Å<sup>0</sup> calculated on the basis of the surface area values) and very imperfect structure because of the presence of large internal porosity as postulated before. The combination of these two may result in the low activation energy necessary for the creep process as observed although the rate controlling mechanism may be volume diffusion. No definite conclusion should be drawn however from this analysis at present.

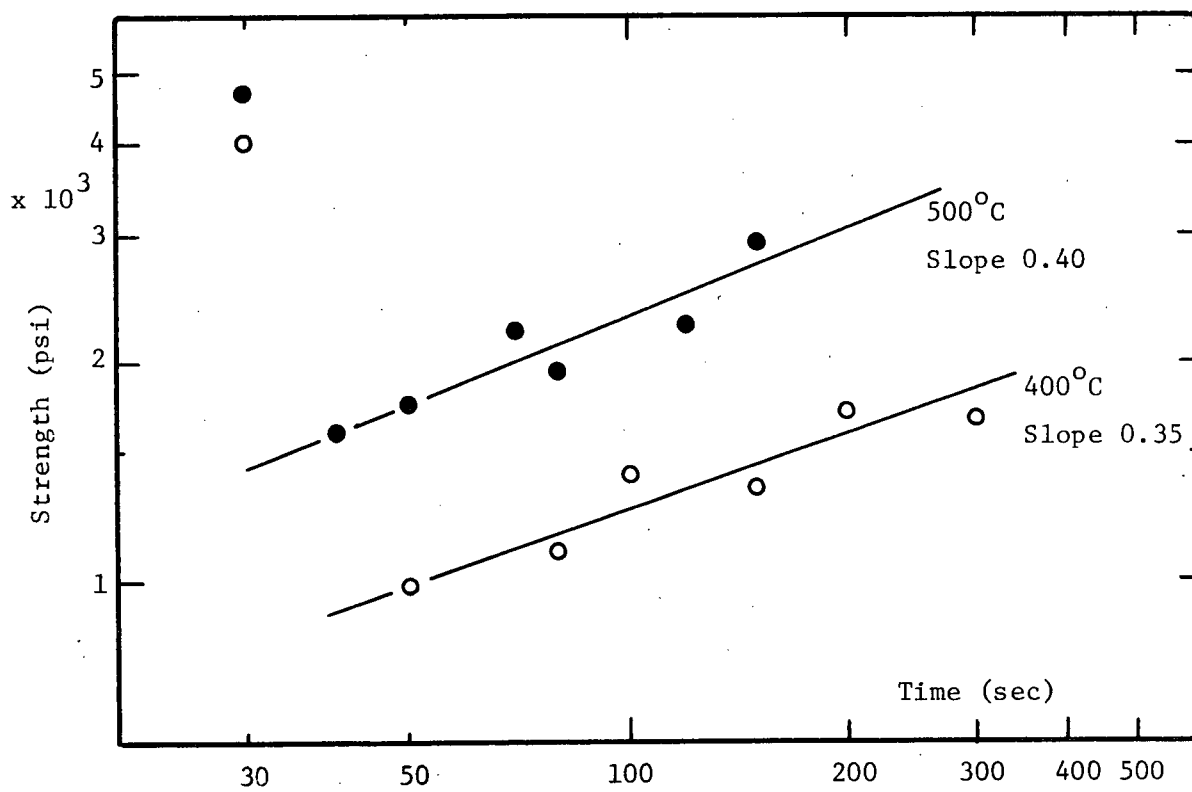


Figure 25 : Log Strength as a function of log time.

#### IV. SUMMARY AND CONCLUSIONS

1. Compressive creep testings of cold compacted colloidal boehmite have been carried out as a function of temperature (in the dehydroxylation temperature range), applied stress and relative density. The compacts have been found to shrink even without any applied stress during the dehydroxylation reaction.
2. The activation energy for the creep process has been determined to be  $9.1 \pm 1.5$  Kcal/mole, which is considerably smaller than the activation energy for the dehydroxylation reaction (42 Kcal/mole), indicating that the rate controlling mechanisms for these two processes are not the same. However, it was experimentally observed that the creep was initiated by the reaction.
3. The creep rate is proportional to the applied stress, although the total creep rate was caused by two factors:  $2\gamma/r$  and the applied stress ( $\sigma$ ), where  $\gamma$  is the surface energy and  $r$  the radius of curvature at the point of contact.
4. The total creep rate ( $\dot{\epsilon}$ ) can be represented by (within the applied stress limit):
 
$$\text{creep rate} = \left[ 0.144 \exp \left( \frac{-9,100 \pm 1,500}{RT} \right) + 2.2 \times 10^{-7} \sigma \right] \text{ sec}^{-1}$$
5. The presence of necks at the points of contact between the aligned fibers has been observed in the electron microscope, thus confirming the driving force ( $2\gamma/r$ ) for the shrinkage, observed in compacts without any applied stress.
6. Equations previously developed, relating the change in length and the strength of a compact (due to neck growth) with time, have been tested with the present experimental data. This analysis indicated although inconclusively, that the rate determining mechanism for the creep process may be volume diffusion.

## V. SUGGESTIONS FOR FUTURE RESEARCH

1. A study of the effect of particle size on the creep rate of boehmite compacts may help in elucidating the mechanisms involved in creep during dehydroxylation.
2. Studies of neck growth between two hemispherical tips of boehmite single crystals would provide information about the nature and mechanism of mass transport during dehydroxylation.
3. In the present work, the dimensions of the specimens were kept approximately constant. The effect of scaling may affect the creep, because of localized pressure of the vapor phase formed during the reaction.
4. All the creep experiments of this study have been done in vacuum. The effect of the partial pressures on the kinetics of the dehydroxylation reaction is known and similarly a study of the effect of partial pressures on the creep behavior during dehydroxylation would help to correlate the reaction and the creep process.

## VI. APPENDIX

### THERMAL EXPANSION OF THE HOLDING FRAME

Due to the fact that the dehydroxylation reaction of boehmite takes place over a wide range of temperatures (350 - 550), and that at 550°C, for example, the reaction is over after 4 minutes (once the test temperature is reached), the furnace has to be heated as fast as possible.

With 9.2 amperes, the heating rate is about 200°C per minute. Since the loading frame is close to the resistance heater, it expands faster than the ram and the dial indicates a contraction as shown in Figure 26(b). After 1500 seconds the expansion of each part is the same and the dial indicator is back to its initial position. The loading frame is fixed to the water-cooled chamber and it seems that it does not continue to expand as much as the ram. The result is an apparent expansion.

Figure 27 shows the relative proportions of the expansion curves compared to the corrected creep curves. Due to the importance of the correction, the creep rates obtained from the corrected curves may be in error by 10%. By repeating many experiments, this value has been found reasonable.

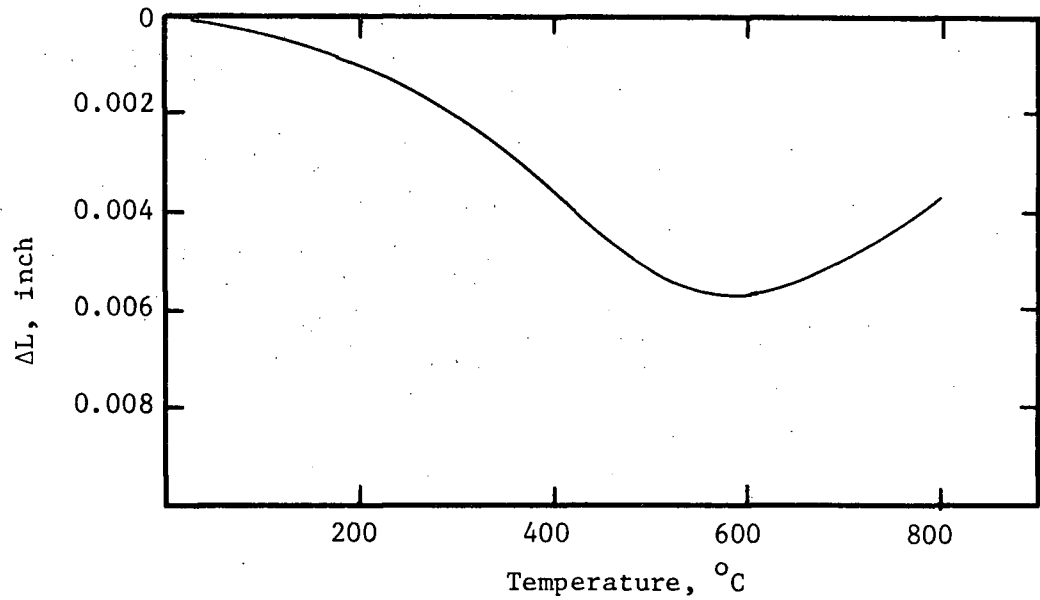


Figure 26(a) : Net dilatation of holding frame during heating rate of  $27^{\circ}\text{C}$  per minute.

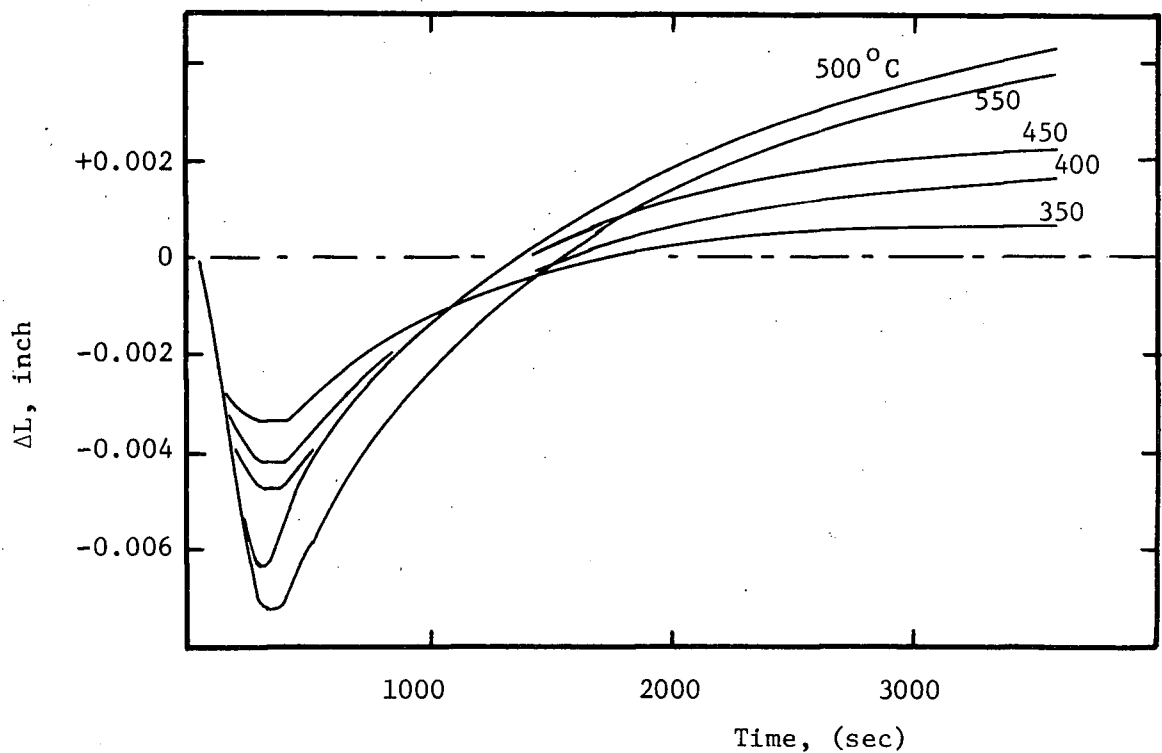


Figure 26(b) : Net dilatation of holding frame during heating ( $200^{\circ}\text{C}/\text{min.}$ ) and isothermal experiment at different temperatures.

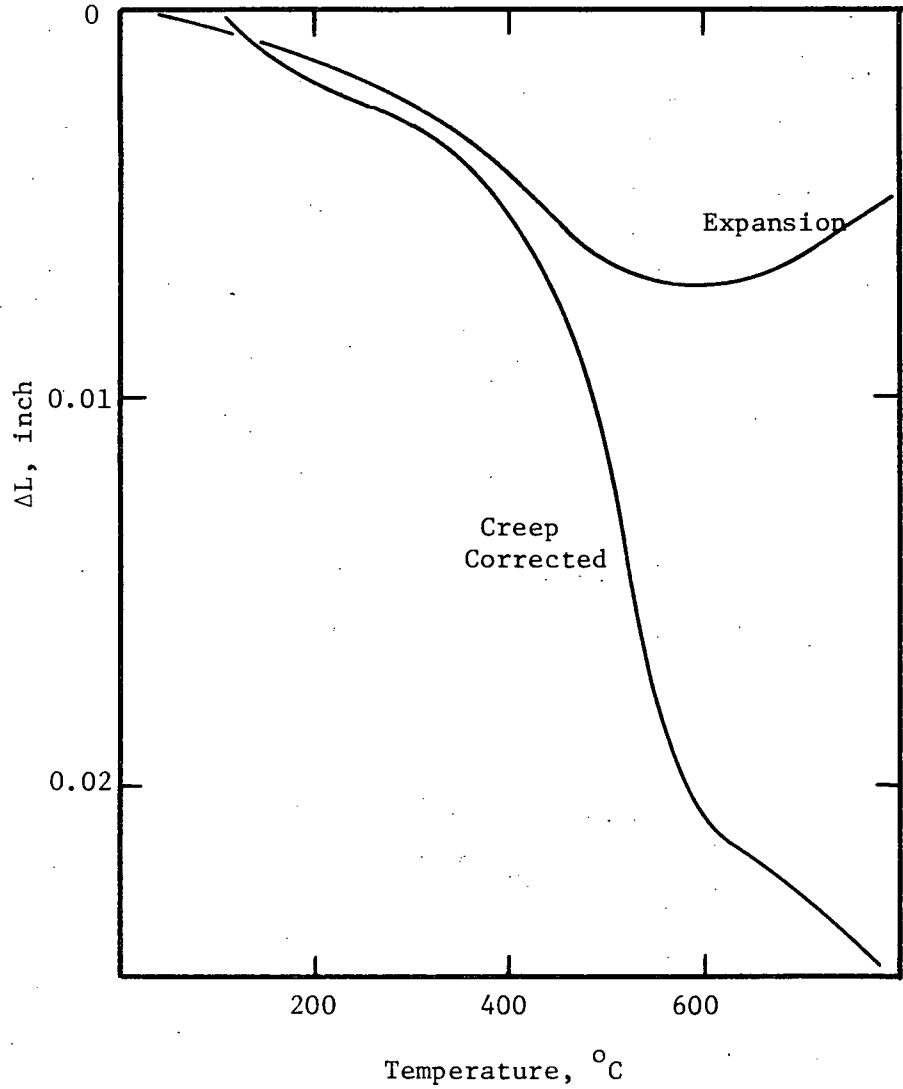
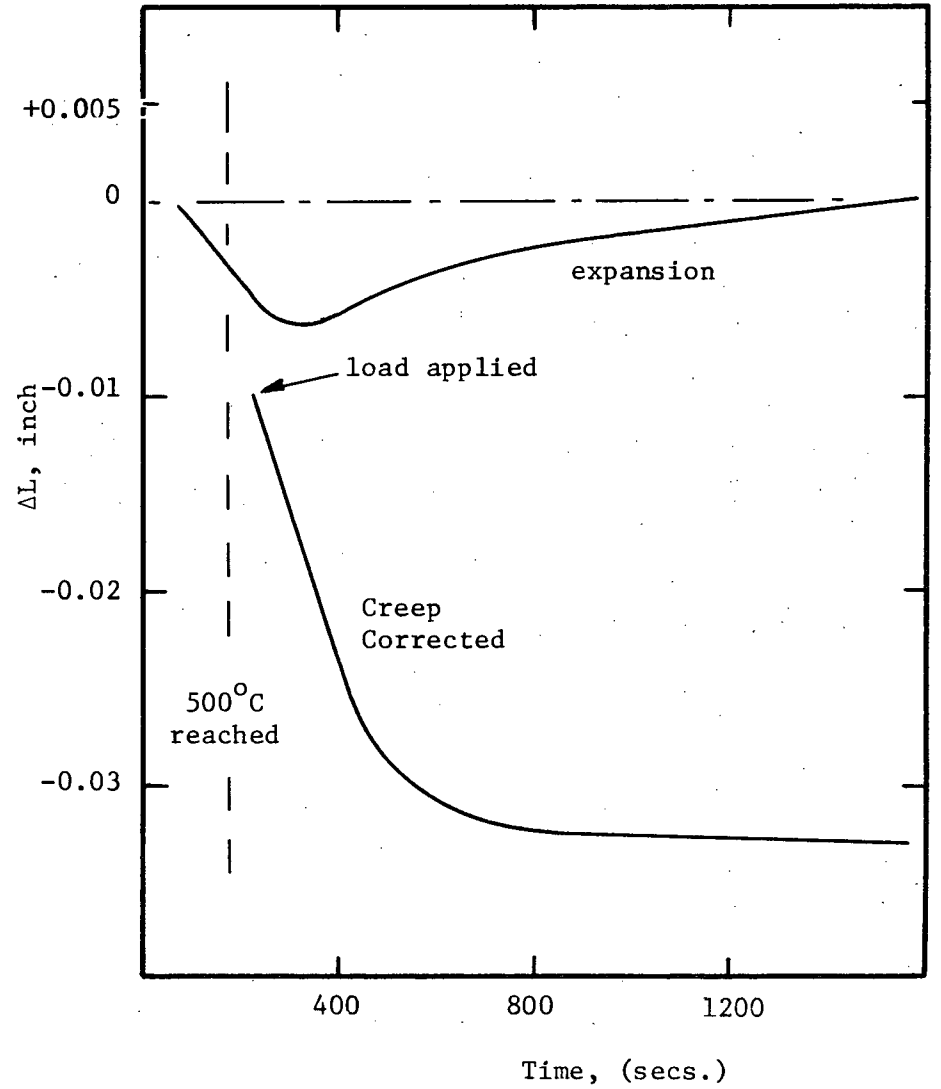


Figure 27(a) : Net dilatation of holding frame compared to corrected creep curve of the compact during heating rate of 27°C per minute.



(b) : Net dilatation of holding frame and corrected creep curve at 500°C under 250 psi.

IV. REFERENCES

1. J.E. Hove and W.C. Riley, "Modern Ceramics," John Wiley and Sons Inc. p. 215 (1965).
2. A.C.D. Chaklader and V.T. Baker, "Reactive Hot-Pressing; Fabrication and Densification of Non-stabilized  $ZrO_2$ ", Am. Ceram. Soc. Bull., 44 [3] 258-59 (1965).
3. (a) A.C.D. Chaklader and L.G. McKenzie, "Reactive Hot-Pressing of Clays," Am. Ceram. Soc. Bull., 43 [12] 892-93 (1964).  
(b) T.G. Carruthers and T.A. Wheat, "Hot-Pressing of Kaolin and of Mixtures of Alumina and Silica," Proc. Brit. Ceram. Soc., 3, 259-73 (1965).  
(c) P.E.D. Morgan and E. Scala, "High-Density Oxides by Decomposition Pressure Sintering of Hydroxides," presented at the Sixty-Seventh Annual Meeting, The Am. Ceram. Soc., Philadelphia, Pa., May 3, 1965 (Basic Science Division, No. 13-B-65); for abstract see Am. Ceram. Soc. Bull., 44 [4] 301 (1965).
4. J.A. Hedvall, Reaktionsfaehigkeit fester Stoffe (Reactivity of Solids), Verlag Johann Ambrosius Barth, Leipzig, (1938), 243 pp. Reprinted by Edwards Inc., Ann Arbor, Mich., 1943; Ceram. Abstr., 17 [4] 164 (1938).
5. A.C.D. Chaklader and L.G. McKenzie, "Reactive Hot-Pressing of Clays and Alumina," J. Am. Ceram. Soc. 49 [9] 477-83 (1966).
6. (a) M. de Long and G.W. Rathenau, Acta Met. 7 246 (1959).  
(b) M. de Long and G.W. Rathenau, Acta Met. 9 714 (1961).  
(c) G.W. Greenwood and R.H. Johnson, Proc. Roy. Soc. A283 403 (1965).  
(d) D. Oelschlägel and V. Weiss, Trans. Quarterly A.S.M. 59 143 (1966).
7. A.C.D. Chaklader, "Deformation of Quartz Crystals at the Transformation Temperature," Nature, 197 791-92 (1963).
8. J.L. Hart and A.C.D. Chaklader, "Superplasticity in pure  $ZrO_2$ ," Mat. Res. Bull., 2 521-26 (1967).
9. P.W. Sunderland and A.C.D. Chaklader, "Deformation during Dehydroxylation of Hydroxides," Mat. Res. Bull., 2 1111 (1967).
10. A.C.D. Chaklader and R.C. Cook, "Kinetics of Reactive Hot-Pressing of Clays and Hydroxides," Am. Ceram. Soc. Bull., 47 [8] 712-16 (1968).
11. R.K. Iler, "Fibrillar Colloidal Boehmite; Progressive Conversion to Gamma, Theta and Alpha Alumina," J. Am. Ceram. Soc. 44 [12] 618-624 (1961).
12. "Alumina Properties," Alcoa Research Laboratory, Technical Paper No. 10, p. 63, Pittsburg, U.S.A. (1960).
13. P.W. Sunderland and A.C.D. Chaklader, "Creep during Dehydroxylation of Magnesium Hydroxide," presented at the Seventieth Annual Meeting,

REFERENCES (continued)

- Am. Ceram. Soc., Chicago, Ill., April 23, 1968 (Basic Science Division, No. 41-B-68).
14. W.D. Callister Jr., I.B. Cutler and R.S. Gordon, "Thermal Decomposition Kinetics of Boehmite," J. Am. Ceram. Soc. 49 [8] 419-22 (1966).
  15. C. Eyraud and R. Goton, "Kinetics of the Thermal Dissociation of the Hydrates of Alumina," J. Chim. Phys., 51 430-33 (1954).
  16. R.S. Gordon and W.D. Kingery, "Thermal Decomposition of Brucite," J. Am. Ceram. Soc., 50 [1] 8 - 14 (1967).
  17. G.W. Brindley and M. Nakahira, "Kinetics of the Thermal Dehydroxylation of Kaolinite and Halloysite," J. Am. Ceram. Soc., 40 [10] 346-50 (1957).
  18. P.E. Evans "The activation energy for grain growth in Alumina," Mater. Sci. Res., 3 345-53 (1966).
  19. W.M. Robertson and R. Chang, "The Kinetics of grain-boundary groove growth on alumina surfaces," Mater. Sci. Res. 3 49-60 (1966).
  20. F. Bueche, "Physical Properties of High Polymers," Interscience Publishers p. 90 (1962).
  21. Vene, Harvo; Makivo, Itsuro, "Kinetics of Butadienne Polymerization in the presence of cobalt catalyst sytems," Kogyo Kagaku Zasshi 71 [3] 418-21 (1968).
  22. M.E. Wadsworth and A.C.D. Chaklader, private communication (1968).
  23. G.C. Kuczynski, "Self-Diffusion in Sintering of Metallic Particles," J. Metals 1 (2), Trans. AIME 185 [2] 169-78 (1949).